Multiprocesses interaction in shaping the seafloor and controlling substrate types, habitats and benthic communities of the Gulf of Cádiz

Pablo Lozano [a*], Luis Miguel Fernández-Salas [b], Francisco Javier Hernández-Molina [c], Ricardo Sánchez-Leal [b], Olga Sánchez-Guillamón [d], Desirée Palomino [d], Carlos Farias [b], Nieves López-González [d], Marga García [e], Juan Tomás Vázquez [d], Yolanda Vila [b], José Luis Rueda [d].

[a] Universidad de Cádiz, Facultad de Ciencias del Mar y Ambientales, Polígono Río San Pedro, 11510, Puerto Real, Cádiz, Spain

[b] Instituto Español de Oceanografía, CO de Cádiz, Muelle Pesquero S/N, 11006 Cádiz, Spain

[c] Department of Earth Sciences, Royal Holloway, University of London, Egham, Surrey TW20 0EX, UK

[d] Instituto Español de Oceanografía, CO de Málaga, Puerto Pesquero S/N, 29640 Fuengirola, Spain

[e] Instituto Andaluz de Ciencias de la Tierra, CSIC-Universidad de Granada, 18100 Armilla, Spain

*Corresponding author: pablo.lozanordonez@gmail.com; Phone number +34 646247198

Abstract

A preponderance of evidence has emerged over recent decades demonstrating the importance of geological oceanographic and biological processes in shaping the seafloor, controlling substrate types and influencing marine habitats and biodiversity. The present research describes how multiple processes interact to shape local seafloor features and determine substrate types and habitats in the middle continental slope of the Gulf of Cádiz. This area represents a unique natural laboratory for studying multiple interacting processes due to

the presence of a contourite depositional system generated by the action of the vigorous Mediterranean Outflow Water (MOW), and influenced by active tectonics that promotes fluid venting activity. Seafloor morphology and substrate types were characterized using a semi-automatic approximation based on geophysical data (multibeam echosounder and parametric subbottom profiler) and ground-truthing by sediment samples and underwater images.

Regional geological and oceanographic processes associated with water mass circulation shape the main morphological features at larger spatial scales while secondary associated oceanographic phenomena (current cores, branches and filaments, eddies, internal waves, etc.) and geological processes (gas venting, mud extrusion, methane-derived authigenic carbonate formation, etc.) are responsible for smaller scale erosional (e.g. channels, marginal valleys), depositional (e.g. dunes), extrusional (e.g. mud volcanoes, pockmarks) and bioconstructed (e.g. mounds, reefs) features. At smaller scales, fluid venting activity and bottom currents generate a wide variety of substrate types and habitats.

Keywords: mud volcanoes; deep-coral; cold venting processes and products; contourite drift; seafloor mapping

1. Introduction

Seafloor morphology and different substrate types result from geological, oceanographic and biological processes interacting at different temporal and spatial scales (Lecours et al., 2015; Micallef et al., 2018). Plate tectonic influence for example spans hundreds of kilometers while bio-construction by benthic organisms occurs at decimeter scales (Camerlenghi, 2018). Advances in remote-sensing imagery contribute to high-resolution mapping techniques and improve understanding of seabed diversity in deep marine environments. In particular, the latest generation of multibeam echosounders combined with seafloor underwater images and more accurate sediment sampling have recently generated higher resolution morphological and seabed type maps. These maps and their correlation with oceanographic data can help further decode formational mechanisms and evolutionary history of seabed morphologies (Lecours et al., 2015; Micallef et al., 2018).

Geological processes such as neotectonics and mud diapirism represent long-term factors that shape the seafloor. These structures form in areas experiencing ongoing collisional tectonics (Kopf, 2002) and in particular as part of accretionary wedges. Examples of this include the Barbados Accretionary Wedge (Brown and Westbrook, 1988), southwestern Taiwan (Chen et al., 2014), the Mediterranean Ridge (Limonov et al., 1996), western Alboran Sea (Pérez-Belzuz et al. 1997) and the Gulf of Cádiz (Somoza et al., 2003; Fernández-Puga et al., 2007; Medialdea et al., 2009). Extrusional (e.g. mud volcanoes) and collapsing (e.g. pockmarks) morphologies are commonly associated with mud diapirism due to pressurized fluid migration (Milkov, 2000; Kopf, 2002, Ceramicola et al., 2018). At smaller scales, microbial activity linked to fluid migration can cause the formation of methane-derived authigenic carbonates (MDACs). These can change seafloor substrate types from soft sediments to hard substrates (Greinert et al., 2001).

Oceanographic processes, such as the persistent action of along-slope bottom currents due to water mass circulation can also promote the formation of a variety of depositional (e.g., drifts) and erosive (e.g. channels) contourite features (Stow et al. 2002; Rebesco et al. 2008, 2014; Stow and Faugères 2008; Esentia et al. 2018). These features can form over vast areas under the influence of vigorous bottom currents. Examples include the continental margins of New Zealand (Carter and McCave 1994), Antarctica (Camerlenghi et al. 1995), Brazil (Faugères et al. 1993), Faroe-Shetland Islands (Masson et al., 2004) and the Gulf of Cádiz (Hernández-Molina et al. 2003; Llave et al., 2007). Other oceanographic processes such as secondary circulation, vertical eddies, internal waves, tides, etc. form in association with water mass circulation. These interact with the seafloor (Rebesco et al., 2014) to generate smaller scale bottom current related features (e.g. Reeder et al., 2011; Belde et al., 2015; Ribó et al., 2016;

Droghei et al., 2016; Yin et al., 2019). The interaction can also promote the development of carbonate mounds commonly formed by scleractinian cold-water corals species (Davies et al., 2011).

Both internal and external processes interact to determine environmental conditions for benthic communities, but specific dynamics between processes that influence habitat and biodiversity remain unclear. This work sought to evaluate the influence of multiple interacting processes in shaping the seafloor, determining substrate types and conditioning habitats and associated biota in the Gulf of Cádiz (GoC). This area represents a natural laboratory for the study of multiple interacting processes due to recent, complex geological activity as well as the local interplay between across- and along-slope oceanographic processes and biological activity. The study area is located along the northwestern continental slope of the GoC, within an area designated as the “channels and diapiric ridges sector” of the Gulf of Cadiz Contourite Depositional System (CDS; Hernández-Molina et al., 2003). This area lies between 300 and 1000 m water depth (wd) and represents a Site of Community Importance ‘Mud volcanoes of the Gulf of Cádiz’ (ESZZ12002) (Fig. 1). This paper presents a detailed high-resolution morphosedimentary analysis of the study area, discusses the onset and evolution of geomorphological features and proposes a model to explain substrate and habitat types based mainly on the links between current velocity and fluid venting.

2. Geological and oceanographic setting

From a geological point of view, the study area is located over the Allochtonous Unit of the Gulf of Cádiz (AUGC). The AUGC is a large olistostromic chaotic deposit composed of Triassic evaporites, Upper Cretaceous red beds, Paleogene limestone and Aquitanian to Tortonian marlstones (Flinch et al., 1996; Maldonado et al., 1999). Its emplacement along the continental margin is associated with compression of the Betic-Rift orogenic belt derived from the westward relative drift and collision of the Alborán Domain with the North African and South Iberian margins (Medialdea et al., 2004; Platt et al., 2013). Changes in tectonic regime since the Upper Tortonian have caused reactivation and novel deformation of the allochthonous unit to trigger vertical migration of plastic materials (mainly Triassic evaporites and Miocene marls) along the main regional tectonic structures (Maldonado et al., 1999; Fernández-Puga et al., 2007) and as large-scale diapiric bodies (Nelson et al., 1993, 1999). Diapiric structures trending NNE-SSW formed and became segmented in several sectors along the slope. Diapirism and related tectonic activity provide adequate fluid migration pathways along fault systems that facilitate the generation of mud volcanoes and pockmarks (Somoza et al., 2002, 2003; Díaz del Río et al., 2003; Palomino et al., 2016). Locally, fluid venting at scales ranging from m to cm promotes the formation of methane-derived authigenic carbonates (MDACs) (Díaz del Río et al., 2003; León et al., 2007).

The AUGC provides an unstable substratum beneath the continental slope which experiences the interplay between along- and down-slope processes. The dominance of along-slope bottom currents due to the Mediterranean Outflow Water (MOW) results in a middle slope terrace morphology consisting of many smaller bottom-current depositional and erosional features (Maldonado et al., 1999; Hernández-Molina et al., 2006, 2016; Llave et al., 2007; Roque et al., 2012; Stow et al., 2013).

The two main water masses influencing the upper and middle slope (Baringer and Price, 1997; García-Lafuente et al., 2007; Carracedo et al., 2016) include the Eastern North Atlantic Central Water (ENACW) which exhibits moderate salinity and temperature values (35.6-36.5, 11-17°C) and the Mediterranean Outflow Water (MOW) which exhibits higher salinity than the ENACW and constant temperature (36.1-36.9, ca. 13°C). Bottom currents associated with these water masses have generated a massive contourite depositional system (CDS) along the middle slope of the GoC (Hernández-Molina et al., 2003; Llave et al., 2007). This system is intersected in its central sector by NE–SW diapiric ridges (Llave et al., 2007; 2011).

The MOW flows northwestward after crossing the Strait of Gibraltar as a vigorous bottom current of up to 2.5 Sv (Barringer and Price, 1997; Sánchez-Leal et al., 2017). At 36.30°N and 7°W, the MOW encounters the Cádiz Diapiric Ridge (CDR, Fig. 2) and then divides into several branches (labeled M1 to M5 from the deepest to shallowest) (Sánchez-Leal et al., 2017) (Fig. 2). The main component of M5 flows northwestward skirting the base of the upper slope with a significant component that is channeled between the CDR through the Gusano Channel (García, 2002; García et al. 2009; Sánchez-Leal et al., 2017). The upper M4 component passes the CDR through a 3 km-wide gorge and flows through the Huelva Channel. The lower M4 hits the CDR and deviates to the southwest until encountering M3, M2 and M1 branches through the Cádiz Channel (Sánchez-Leal et al., 2017) (Fig. 2). MOW and is interface with the ENACW influence the rest of the area located between the main MOW branches (Sánchez-Leal et al., 2017).

3. Methodology

This work mapped seafloor morphology and substrate types using a semi-automatic approximation based on geophysical data (multibeam echosounder and very high resolution seismic profiles). Data were validated by rock and sediments samples and visual interpretation of submarine imagery (Fig.1b) as well as by near-bottom oceanographic observations (Fig. 2).

3.1. Data acquisition

Data were obtained during eight oceanographic expeditions that were part of research projects LIFE+ INDEMARES/CHICA (2011 and 2012) and ISUNEPCA (2014 to 2019). Bathymetric and backscatter data were acquired with a Kongsberg Simrad EM-300 and EM-710 multibeam echosounders and processed with Caris Hips and Sips software to produce a 15 × 15 m bathymetric and backscatter grid model of the study area.

Very high resolution seismic reflection profiles were acquired with a TOPAS PS018 subbottom profiler. The system uses a primary frequency of 16-20 kHz and a secondary frequency of 0.5-4 kHz. Pre-amplifying, TVG amplifying and band-pass filtering were applied to the acquired data and the results were interpreted using IHS Kingdom software.

A total of 46 sediment samples (Fig. 1b) were collected using box-corers and Shipek grabs in order to characterize sediment texture and validate the acoustic classes defined by analysis of backscatter models.

High-resolution underwater images were collected by the Remotely Operated Vehicle (ROV) LIROPUS 2000 and the Underwater Camera Sleds (UCS) APHIA 2012, HORUS and TRISION. Underwater images were obtained with high precision submarine navigation, capturing images between 0.5 and 2.5 m from the seafloor, during 1–3 hour (ROV) and 0.2–1 hour (UCS) transects. The mean explored distances were between 223 and 1025 m for ROV transects and between 80 and 379 m for UCS transects. Measurement of some seafloor biological (e.g. densities, colony size, coverage) and geological features (e.g. size of MDACs, coral rubble coverage) observed in each transect were conducted using laser pointers for scale. Identification of key species was possible using the information provided by samples collected in the same areas using different methods such as box-corer (BC) (ca. 0.09 m^2 sampling area and mostly targeting infaunal organisms from sedimentary habitats) and beam-trawl (BT) (ca. 2000 m^2 and mostly targeting epifaunal and demersal organisms from sedimentary and non-sedimentary environments).

We used interpolated fields of near-bottom hydrographic and velocity observations taken from Sánchez-Leal et al. (2017) to evaluate the oceanographic setting.

3.2. Morphosedimentary characterization

Mapping and further morphological analyses were conducted with the ArcGIS software (ESRI, Redlands, CA) using bathymetry first derivatives such as slope (Fig. 3a) and aspect (Fig. 3b) variables as well as the Benthic Terrain Modeller (BTM) geoprocessing tool. The BTM was utilized to calculate standardized bathymetric position indexes (BPI) (Figs. 3c and 3d). These layers measure height differences between a focal point and the average calculated over surrounding cells within a defined radius. The two different BPI-pairs produced included a broad-scale BPI (b-BPI; 40 units for the inner radius, 80 units for the outer radius and scale factor 1200) (Fig. 3c) and a fine-scale BPI (f-BPI; 8 units for the inner radius, 16 units for the outer radius and scale factor 240) (Fig. 3d). These scales were chosen to help capture broad-scale (e.g., channels) and fine-scale (e.g., dunes) seafloor features identified by examination of the bathymetry. Backscatter values (Fig. 3e) were processed using a Geocoder algorithm by Caris Hips and Sips software. A substrate types map was made interpreting reclassification of backscatter into acoustic classes (Fig. 3f).. Samples and underwater images helped validate the results.

Sediment samples were categorized by weight percent of gravel, sand and mud, and plotted on Folk (1954) ternary diagrams following a modification more adequate for benthic habitat studies (Long, 2006). All gravel containing sediment classes are merged into a "mixed sediment" class and all gravel classes are merged into "coarse sediments". New classes have been defined based on underwater image analyses. These included "rock with coarse sediments", "rock with mixed sediments", "rock with sand", etc.

To describe the morphosedimentary characteristics, the study area was divided into several zones based on its primary physiographic characteristic(both diapiric ridges which intersect the study area in a NNE-SSW direction and three main channels which cross the study area in a WNW-ESE direction). Thus, the proximal zone lies east of the Cádiz Diapiric Ridge (CDR), the central zone lies between the CDR and Guadalquivir Diapiric Ridge (GDR), the proximal zone lies west of the GDR, the northern sector lies north of Gusano Channel, the mid sector lies between Gusano Channel and Huelva Channel and southern sector lies south of Huelva Channel (Figs 2 and 4).

4. Results

The study area hosts an irregular seafloor relief containing a number of features that can be grouped into five morphological types. These include shale tectonic features, features linked to fluid migration, depositional features and erosional features (Fig. 4). Every morphological type displays different substrates, from rocky bottoms to muddy deposits. At smaller scale, morphological types also host a variety of bedforms, habitats and benthic species.

4.1. Shale tectonic features

Related to mud diapirism, several diapiric ridges and isolated diapirs outcrop the seafloor.

4.1.1. Diapiric ridges

Two diapiric ridges, about 30 km in length occur in the study area, the Guadalquivir Diapiric Ridge (GDR) and the Cádiz Diapiric Ridge (CDR) (Figs. 1 and 4). Both of these features are nearly linear but are bisected by channels and valleys in several sectors.

Guadalquivir Diapiric Ridge (GDR)

This ridge appears at 450 m wd in the northeastern part of the study area and runs southwest until its western terminus at 800 m wd (Fig. 4). Its northwestern flank exhibits higher slopes (20-35°) and higher backscatter values (between -12 and -8 dB) than its southeastern flank (slopes of 2-10° and backscatter values between -20 and -16 dB). The GDR can be divided into three different sectors (Fig. 4) referred to as the northern, mid and southern sectors.

The GDR's northern sector is located north of the Gusano Channel and is divided into three parts. The northern part of this sector has a relatively flat summit hosting five cone-like mounds (Figs. 4 and 5a). The flat summit is mainly covered by muddy sand deposits embedded with different seapens (e.g. *Funiculina quadrangularis*, *Kophobelemnon stelliferum*) (Fig 5b). Mounds show higher backscatter values (between -19 and -14 dB) than the adjacent seafloor. The largest mound has a summit reaching 390 m wd for a total of 28 m relief and a circular base 300 m in diameter. Summit areas consist primarily of coral rubble inhabited by small gorgonians (mainly *Bebryce mollis* and *Swiftia pallida*) (Fig. 5c).

The GDR's mid sector lies between the Gusano and Huelva channels. It displays continuous, linear relief (Figs. 4 and 6a), extends 8.2 km in length, spans 0.8 km in width and reaches 150 m in height. A narrower part of the mid sector to the south runs almost parallel and overlaps the main feature (Figs. 6a and 6b). The top is covered by mixed sediments (mainly gravelly sand) with a high density of crinoids (*Leptometra phalangium*) (Fig. 6c). The western flank exhibits higher backscatter values (between -6 and -14 dB) indicating a coarse clastic surface with some sessile (mainly sponges like *Phakellia* sp.) and mobile species (mainly the crinoid *Antedon* sp.) (Fig. 6d).

The GDR's southern sector is located south of the Huelva Channel and is segmented into five parts (Fig. 4) with reliefs ranging from 100 to 160 m in height. All of these have higher slopes and backscatter values along their northwestern flanks than their southeastern flanks. Samples and underwater images were not acquired for this sector.

Cádiz Diapiric Ridge (CDR)

The CDR crops out at 460 m wd and runs south of the Tofiño Channel until it reaches the northern margin of the Cádiz Channel at 880 m wd. This feature can be divided into three different sectors (Fig. 4) referred to as the northern, mid and southern sectors. .

The northern sector lies north of the Gusano channel and consists of smaller segments of different dimensions ranging from 100 to 2700 m in length and 20 to 200 m in height (Figs. 4 and 7a). A narrow and isolated crest appears along the northeastern margin of the Tofiño Channel at 450 m wd. This crest is 1900 m long and 117 m wide. Its substrate consists of exposed slabs, crusts and chimneys bottoms that lack evidence of benthic fauna (Fig. 7b). An E-W oriented crest of about 2700 m in length appears between Tofiño and Gusano channels. The southern flank exhibits a ramp-like shape. Its substrate consists primarily of sand with patches containing boulders and MDAC slabs (Fig. 7c). Hard bottom areas are colonized by some large unidentified desmosponges and echinoids (*Cidaris cidaris*).

In its proximal zone at the beginning of the Gusano Channel, the mid sector shows two crests around 600 m in length and 400 m in width. Their summits reach 320 m wd and 365 m wd respectively. The flanks around both crests exhibit steep slopes (45 to 53º) and high backscatter values (-10 to -6 dB). Their substrates are dominated by large boulders with some patches of sand colonized by large gorgonians (*Callogorgia verticillata*) (Fig. 7d). The proximal zone also hosts two circular mounds ranging from 300 to 450 m in diameter and 50 to 100 m in height with substrates dominated by coral rubble (Fig. 7g). The distal zone between Gusano Channel and Huelva Channel is characterized by low to medium backscatter values (-22 to -15 dB) and dispersed circular to elongate areas with high backscatter values (-10 to 6 db). This area hosts more than 20 isolated mounds ranging 100 to 300 m in diameter and 5 to 15 m in height (Figs. 7a and 7f). Substrate on top of mounds consists of semiburied MDACs (Fig. 7e). Areas surrounding the mounds consist primarily of soft sediments. The large hexactinellid sponge *Asconema setubalense* inhabits the MDACs while the seapen *Kophobelemnon stelliferum* and the small sponge *Thenea muricata* inhabit unconsolidated sediments.

The southern sector of the CDR is located along the southern margin of the Huelva Channel and divides into two parts (Figs. 4 and 8). The northern part is a set of elevations with a summit at 365 m wd rising up from 800 m wd at the basal part of the channel. The southern part is 10 km in length and 3 km in width.,It follows the edge of the Cádiz Channel and exhibits high backscatter values (-11 to -2 dB) and a crested surface (Fig. 8a). Seismic profiles (Fig. 8b) revealed a suite of up to 30 buried and exposed mound features along the crest of the ridge (Fig. 8a). The mounds occur between 700 and 800 m wd and display reliefs of up to 40 m. These exhibit elongation in a NE–SW direction and extend about 4 km in length. Valleys between crests host large amounts of coral rubble (Fig. 8c) and the flanks show live colonies of *Madrepora oculata* (Fig. 8d).

4.1.2. Isolated diapirs

Three isolated diapirs appear along the northwestern flank of the GDR's northern sector (Fig. 4). The Elcano diapir represents the largest of these features. It exhibits an elliptical shape with a base located at 520 m wd and 60 m relief. A prominent depression appears along its NW flank. The summit consists primarily of sandy mud sediments with embedded seapens and patches of sand and gravelly sand substrate.

Another diapir, La Pepa, exhibits a semicircular shape. Its base lies at 510 m wd from which it rises up to form 25 m of relief from the adjacent bottom. The seabed consists primarily of sandy mud sediments embedded with seapens (mainly *K. stelliferum*, *F. quadrangularis*). The Bicentenario diapir also has an elliptical shape. Its base lies at 515 m wd and rises up to 30 m of relief. The bottom is covered by sandy mud sediments that are partly bioturbated and which contain shell remains.

4.2. Features linked to fluid migration

4.2.1. Mud volcanoes (MVs)

Four conical MVs (Gazul, Pipoca, Anastasya and Tarsis, Fig. 4) located in the study area between 450 and 620 m wd were previously described in Palomino et al. (2016). The Gazul MV (Figs. 1b and 4) exhibits a subcircular shape and reaches a height of 107 m. The top as well as the northern and northwestern flanks show high backscatter values (-15 to -19 dB) due to their gravel substrate (Fig. 9a), MDAC and cold-water coral banks. These consist primarily of *M. oculata, D. cornigera* and *L. pertusa* along with a wide variety of sponges and other hard substrate epifauna (Fig. 9b). Its southern and southeastern flanks exhibit low backscatter values (-22 to -28 dB) associated with sandy mud sediments and the presence of seapens. Two depressions located north and northwest of the MV trend in a NW direction (Fig. 9a). These deepen up to 12 m and occupy ~2 km^2 area. The northern depression includes two local outcrops exhibiting planar, semicircular shapes and high backscatter values (-13 to -17 dB) likely due to MDAC crusts colonized by large habitat-forming species. Gravelly sand deposits surround these outcrops. The northwestern depression also contains outcrops forming several NW-SE oriented parallel ridges extending 700 m in length. In the middle of the depression, the seafloor is dominated by gravelly sand with some solitary scleractinians (*Flabellum chunii*) (Fig. 9c).

Anastasya MV (Figs. 1b and 4) exhibits 100 m of relief. Its summit appears as a top-dome with low backscatter values (-23 to -26 dB) surrounded by a caldera-depression (Fig. 9d) with moderate backscatter values (-15 to 20 dB). The top-dome is dominated by fluid-rich mud with some microbial mats (Fig. 9e) and chemosymbiotic infauna (mainly the bivalves *Solemya elarraichensis* and *Lucinoma asapheus*). The seafloor of the caldera-depression consists of gravelly mud with small rocky outcrops (Fig. 9f). Several mud flows surround the cone, exhibiting some overlap and relatively low backscatter values (-26 to -29 dB). The local seafloor here is sandier and hosts a relatively high density of burrowing megafauna and a lower density of seapens consisting mostly of *K. stelliferum*.

Pipoca MV (Figs. 1b and 4) has an elliptical shape and a relief of 120 m. A large mud flow, characterized by very high backscatter values (-6 to -9 dB), runs from the summit down the southwestern flank and debouches into the Huelva Channel. The seafloor consists of gravelly sand deposits, covered by high-density fields of the crinoid *L. phalangium*, with occassinal boulders colonized by gorgonians (e.g. *Acanthogorgia hirsuta*) and sponges (e.g. *A. setubalense*). The northern flank exhibits smaller and less reflective (-18 to -20 dB) mud deposits. In this part, the MV is surrounded by various depressions that connect with the western terminus of the Gusano Channel (Fig. 4).

Tarsis MV (Figs. 1b and 4) reaches a height of 40 m and is partially surrounded by a rim depression. Both the summit and related depression display patches with high backscatter values (-8 to -10 dB). The summit contains gravelly sand deposits, covered by fields of *L. phalangium* together with different species of pennatulaceans (*F. quadrangularis, Pennatula* *aculeata,*) and some bamboo corals (*Isidella elongata*). The base is dominated by muddy sand deposits colonized by *K. stelliferum*.

4.2.2. Mud Volcano/diapir complexes

Two mud volcano/diapir (MV/D) complexes, Chica and Geraldine (Fig. 4), occur in the study area between 700 and 850 wd. Previously described by Palomino et al. (2016), Chica MV/D (Fig. 4) consists of 10 conical mounds with very high backscatter values (-4 to -8 dB). It is flanked to the East by a depression that is 50 m deep, 1.1 km long and 0.6 km wide. Mound substrate consists of irregular and massive MDACs colonized by gorgonians (*Viminella flagelum and C. verticillata*) and other sessile species like sponges. Gravelly sand ripples and some MDAC fragments make up the seabed surrounding the mounds.

Geraldine MV/D (Fig. 4) is a diapiric outcrop with two E-W oriented ridges formed by a series of isolated mounds. These reach lengths of 4 and 6 km (Figs. 10A and 10b). Mud breccias with abundant coral rubble detected in samples collected from the mounds confirmed their MV designation (Fig. 10c). These features also host live colonies of cold-water corals (CWC) such as *L. pertusa* (Fig. 10d). A depression surrounding the southern and western flanks reaches a maximum depth of 200 m from the base of the diapir. This feature hosts live CWC including black corals (*Leiopathes glaberrima*) (Fig. 10e).

4.2.3. Pockmarks

The study area includes two pockmark fields and several isolated pockmarks (Figs. 4, 5, 6 and 9d). All of these exhibit circular shapes with diameters of 60 to 250 m and a vertical incision between 2 and 12 m deep. Between the GDR and CDR, north of the Huelva Channel, eight pockmarks appear between 600 and 570 m wd. These assume circular shapes with diameters between 140 and 250 m. Vertical profiles are V-shaped with 2-7 m incision. Another pockmark field occurs around Anastasya MV (Fig. 9b). This field consists of eight pockmarks clustered together 1.5 km from the southwestern flank of the MV. Three remaining pockmarks lie close to the base of Anastasya MV. All of these exhibit circular shapes with diameters between 62 and

214 m and 2-12 m incision. Only one pockmark north of Anastasya MV (Fig. 9d) exhibits different backscatter values relative to those of adjacent flat areas. Several isolated pockmarks appear near the CDR (Figs. 5a and 6a) and close to the Bicentenario diapir.

4.3. Depositional features

4.3.1. Sedimentary drifts

Approximately 70% of the study area is flat and covered by soft sediments. These represent large contourite sheet drifts (Fig. 4) previously described in Llave et al. (2007). Underwater images and backscatter data show a variety of sediment types from sandy to muddy deposits along the seafloor and along upper surfaces of these drift deposits.

In the distal zone of northern sector, northwest of the GDR, mud and sandy mud make up an extensive 225 km^2 area between 490 and 575 m wd. Soft sediment in this area is highly bioturbated. Some areas show homogenization and trawling marks with some seapens and burrowing megafauna (mainly decapods). Areas north of the CDR to the northern limit of the study area (proximal and central zone-northern sector) consist of sand and mixed sediments with numerous ripples.

In the central zone-mid sector which lies between both diapiric ridges, the most common texture is muddy sand but gravel becomes more prevalent close to the ridges while sand becomes more prevalent close to channels. In the proximal zone east of the CDR, flat areas are dominated by gravelly sand and gravelly mud sediments. Gravel consists primarily of bioclasts.

4.3.2. Dunes

Several large-scale bedforms have been designated as ‘dunes’ following the classification of Ashley (1990) according to primary descriptors of shape (i.e. 2D or 3D) and size (spacing and height). The 2D dunes exhibit flat bounding surfaces of crossbedding while 3D dunes exhibit scoured or trough-shaped bounding surfaces. All dunes identified in the study area categorize as large (10-100 m wavelength and 0.75-5 m height) or very large (>100 m wavelength and >5 m height).

2-Dimensional very large dunes

Three fields with very large dunes occur along margins of channels or marginal valleys (Figs. 4, 7a and 8a). These dunes are generally 2D and without bifurcations. Their axes run parallel to each other and decrease in size with increasing distance from the channel axis (Fig. 8e).

A set of six dunes appears at the southern margin of the Gusano Channel and west of the CDR (Figs. 4 and 7a). Located between 520 and 550 m wd, these dunes exhibit axes oriented in a north-south direction but with a slight asymmetry and running oblique to the axis of the channel. Their wavelengths range from 320 and 415 m, while their lengths range from 360 and 540 m. Their heights reach 20-30 m with nearly symmetric stoss and lee slopes. The bottom is dominated by sandy mud sediments without superposed bedforms but hosting low densities of seapens (*F. quadrangularis*) and sea anemones (*Actinauge richardii*).

Along the southern margin of the Gusano Channel before it crosses the GDR from west to east, three dunes exhibit curved crests oriented in a primarily NNE-SSW direction (Fig. 4). These occur between 525 and 550 m wd with heights of 8 and 10 m, lengths of 1300 and 2400 m and wavelengths ranging between 175 and 325 m that becomes greater with the distance to the flank of the channel.

Another dune field occurs between the Huelva and Cádiz channels, at the head of a funnel-shaped marginal valley at 620 and 650 m wd (Fig. 8a). It hosts seven arc-shaped dunes that range from 5 to 18 m in height, 1200 to 1350 m in length and have wavelengths from 450 and 600 m. Waves decrease in height and increase in distance from each other with increasing distance from the head of the marginal valley. All of these features exhibit symmetric stoss and lee slopes (Fig. 8e). Bottom areas are dominated by sandy mud sediments without superimposed bedforms (Fig. 8f) but hosting high densities of seapens (*K. stelliferum*). The seismic profile (Fig. 8e) shows a sedimentary sequence recording the evolution of this dune field. The oldest phase shows dunes with a very large wavelengths eand low heights evolving vertically into dunes with shorter wavelengths and higher heights.

3-Dimensional large and very large dunes

There are seven fields of 2D large to very large dunes exhibiting scoured and superimposed waves. Five of these occur within the Cádiz Channel and only one inside the Huelva Channel (Fig. 4). The largest dune field occurs in the proximal zone east of the CDR along the eastern limit of the study area. With heights between 6 and 13 m and wavelengths of about 100-150 m, these categorize as very large dunes. All of these features exhibit an asymmetrical profile with lee sides steeper than stoss sides. The bottom is dominated by sandy sediment with ripples and abundant bioclasts (Fig. 8g).

The rest of the 3D dune fields in the Cádiz Channel cover areas ranging from 2.2 and 5.1 km^2. Dunes range 3 and 5 m in height and exhibit wavelengths ranging from 60 to 100 m. The Huelva Channel dune field covers 1.1 km^2 area. Ranging 3 to 10 m in height and 80 and 150 m in wavelength, the waves categorize as large to very large. All of these exhibit medium to high backscatter values that correspond with sand and gravelly sand sediments.

4.4. Erosional features

4.4.1. Channels

Four staggered channels crisscross the study area. The two main channels (Huelva and Cádiz channels) strike in a primarily WNW direction. Of the two other smaller channels, the Gusano Channel follows a sinuous E - W path while the Tofiño Channel runs N to NW (Figs. 1b, 4 and 11).

Huelva Channel

The Huelva Channel axis runs between 566 and 860 m wd and exhibits considerable variation in width (1.2 to 3.6 km) and incision (60 to 310 m). Consisting of three different zones, it crosses both the CDR and GDR. Upstream of CDR intersection, the proximal zone exhibits moderate backscatter values (-19 to -23 dB) and surface substrates consisting of sandy sediments imprinted with ripple marks. When the channel crosses the CDR, it incises and erodes an area of very high backscatter values (-2 to -10 dB).

The channel reaches its maximum width and incision in the central zone between ridges. The pronounced northern margin of the channel contains a terrace that reaches slopes of 17°. The southern margin exhibits more gentle features. Backscatter values progressively decrease westwards (from -10 to -22 dB) and the seabed consists primarily of muddy sand sediments, minor bioturbation and embedded seapens. The channel crosses the GDR in the distal zone, where it turns slightly to the north and then to the west to skirt around the ridge and Pipoca MV. In this region, backscatter increases from -20 to -10 dB and the sediment becomes sandier.

Cádiz Channel

The Cádiz Channel intersects the study area from east to west along an axis that lies between 710 and 1000 m wd. With a width that ranges from 2.5 to 10 km, this channel is the widest channel of the study area. It incises 90 to 290 m of verticat. In the proximal zone east of the CDR, the channel hosts very large 3D dunes (see description below). The main axis of the channel becomes wider in the central zone after it crosses the CDR. The right margin consists of 40 and 60 m high terraces. The channel exhibits moderate to high backscatter values (-10 to -14 dB) that correspond with gravelly sand with patches of rocky outcrop giving very high backscatter values(-3 to -6 dB).

Gusano Channel

The Gusano Channel runs 28 km in length and spans 500 to 1800 m in width. Its main axis lies between 480 and 700 m wd. It initially appears east of the CDR and terminates west of the GDR. Between these points, its expresses three different zones and crosses both diapiric ridges.

The initial 12 km length (from the east) of the channel lies in the proximal zone. Striking in a SE-NW direction, the channel crosses the CDR and incises between 40 and 80 m of seafloor. The channel in this zone exhibits medium to high backscatter values (-19 to -10 dB) that correspond to gravelly sand deposits (Fig. 7a). Patches of higher backscatter values (-10 to -5 dB) also appear. The central zone spans the proceeding 3 km (westward) to incise < 20 m of seafloor after the channel crosses the CDR. The channel spans up to 1.5 km width. The morphology of the channel is only appreciated checking the b-BPI that shows its continuity. The seabed exhibits low backscatter values (-23 to -16 dB). These however exceed those of surrounding flat areas characterized by muddy sand sediments.

In the distal zone, prior to reaching the GDR, the channel becomes conspicuously tortuous over a 10 km stretch exhibiting pronounced bends while traversing diapiric ridges. The channel opens towards the west near Pipoca MV. The incision at this point reaches 200 m. Meanders in the channel include terraces ranging from 30 100 m in height. The terraces consist of compacted mud while the channel seafloor is dominated by sandy ripples with bioclasts and dense crinoid-dominated aggregates (probably *L. phalangium*).

Tofiño Channel

Tofiño Channel is a narrow channel reaching 10.7 km in length and 0.6 km in width. The channel begins in the northern sector of the CDR. Its axis lies between 470 and 505 m wd and incises between 15 to 40 m of seafloor. Along its NE margin, isolated outcrops and a 30 m escarpment confer a steep appearance on the channel. The substrate exhibits sandy deposits with abundant ripples.

4.4.2. Marginal valleys

Marginal valleys appear as channel features behind linear relief. Most of these features are abrupt, elongate and narrow channels running parallel to western flanks of the ridges. They span 1.5 to 13.5 km in length and 100 to 600 m in width (Fig. 4). The longest one follows the western flank of the GDR's northern sector over a 13.5 km stretch until it reaches the Gusano Channel (Figs. 5a and 6a). Its axis lies between 490 and 700 m wd and its width varies from 200 to 1100 m. This feature incises 15 to 160 m of seafloor. A semicircular depression appears along the axis of this marginal valley. It spans ca. 3 km in diameter and incises 160 m of seafloor (Fig. 5a). Sliding marks along its margins and the channel is dominated by muddy sediments .

Other marginal valleys assume a funnel-shaped form wherein canyon heads terminate in narrow channels (e.g. fig. 8). These types of marginal valleys have only been detected within the CDR. They range in length from 1.9 to 8 km and span widths of 1.1 to 5.1 km. The largest feature follows the western flank of the southern sector of the CDR over an 8 km stretch until it reaches the Cádiz Channel. The widest part consists of three semi-circular structures that resemble a canyon head and host terraces up to 50 m high. These converge into a single, narrow channel that is 500 m in width and incises 160 m of sediment (Fig. 8a).

4.4.3. Isolated depressions

Several circular and semicircular concave features are dispersed around flat areas or in the middle of channels. Four isolated depressions appear in the central zone of the mid sector north of the Huelva Channel (Fig. 4). These exhibit smooth flanks but do not present backscatter values that differ from adjacent flat areas comprised of sandy mud substrate. Two depressions assume a semi-circular shape (700 and 500 m in diameter; 15 and 10 m incision beneath adjacent bottoms). The other two depressions exhibit elongate shapes (1.8 and 1.1 km in length; 5 and 6 m incision beneath adjacent bottoms).

An elliptical depression appears within the Huelva Channel southeast of the GDR (Fig. 4). This feature has a semi-major axis of 3.7 km, a semi-minor axis of 2.5 km and incises 60 m of sediment. The south, east and especially southeast flanks show a steep margin with high backscatter values that correspond to rock and gravelly bottom areas. Northern and western flanks show a smooth margin composed of sandy mud bottoms.

An additional isolated depression appears in the distal zone-mid sector, northwest of the GDR and between the terminus of the Gusano Channel and Pipoca MV (Fig. 4). Its semi-major axis extends 2.2 km in length, its semi-minor axis extends 0.8 km in width and the feature incises 24 m deeper than adjacent bottoms. This feature exhibits a steep margin and does not show differences in backscatter values relative to adjacent flats consisting of muddy sand substrate.

A semi-circular depression occurs 0.8 km northwest of Pipoca MV's base and 1.5 km north of the Huelva Channel (Fig. 4). It spans 1.7 km in diameter and extends 90 m in depth. It has steep north and northeast flanks showing high backscatter values that correspond to gravelly deposits. Finally, an irregular shaped depression with steep margins appears at 40 m depth. It is located southwest of the Huelva Channel and northwest of the GDR (Fig. 4).

5. Discussion

5.1. Origin of morphological features

5.1.1. Features associated with shale tectonics and extrusion processes

The present bathymetric expression of mud diapirism is aligned mostly NNE-SSW (Fig. 4). These features constitute the deformational front of the accretionary wedge and their morphology results from different tectonic regimes. Tectonic initiation of linear diapiric ridges occurred due to gravitational ascent of marls related to extensional collapse (Flinch et al., 1996; Maestro et al. 2003). These bodies were later segmented and rotated in several different sectors (Llave et al., 2006, 2007). García et al. (2009) explained segmentation of diapiric ridges in different sectors according to movement along dextral WNW-ESE-trending faults. Similar segmentation has also been documented along the Portuguese and Spanish margin (Pinheiro et al., 2003; Medialdea et al., 2004; Rosas et al., 2009). These faults coincide with several MVs and MV/D complexes in the study area (Fig. 11). The Anastasya MV lies near the gap between the GDR's northern and mid sectors. Tarsis and Pipoca MVs lie within the gap between the GDR's mid and southern sectors. This is also true for Chica and Geraldine MV/diapir complexes (Fig. 4) indicating that faulting controls fluid migration up to the seafloor (Fig. 11). Similar mechanisms have been described from other areas of the GoC (Medialdea et al., 2009; Rosas et al., 2009).

Other types of geomorphological features such as the pockmarks and depressions form from migration of overpressured fluids and further sedimentary collapse. Pockmark fields occur in the contourite drift between the Gusano and Huelva channels and both diapiric ridges (Fig. 4) and also surrounding Anastasya MV (Fig. 9d). Only pockmarks surrounding Anastasya MV display differences in backscatter values relative to the surrounding seafloor. As such it could represent an indicator of past (e.g. MDACs or skeletal remains of chemosymbiotic organisms on the seafloor) and/or present (e.g. fluids trapped on the sediment) activity. Similar mechanisms influence pockmarks observed in the Mediterranean Sea (e.g. Gela Basin pockmark field) (Taviani et al., 2013). These pockmarks may arise from focused gas migration along faults (Palomino et al. 2016) which decreases interstitial fluid pore pressure and causes seafloor surface collapses. Similar mechanisms have been proposed to explain the formation of the isolated depressions, which may arise from more intensive and punctuated gas migration. The irregular shape of these depressions may additionally indicate the effect of bottom currents re-shaping these features. Such a mechanism has been proposed for similar depressions in other areas (García et al., 2016; Yin et al., 2019). The MVs and MV/D complexes leeward of the depression also arise from interacting effects of fluid migration and bottom current action as previously proposed by Palomino et. al. (2016). The dominant process in this case is likely bottom currents sculpting the depressions.

5.1.2. Features associated with oceanographic processes

A) Channeled drift

The effect of Mediterranean Outflow Water (MOW) and its interaction with tectonically-influenced features generates the main depositional and erosive features described here. Following dextral WNW-ESE-trending faults, the MOW has eroded several along-slope channels (Fig. 11) where bottom currents enhance their velocity (Fig. 2). These channels appear staggered and form terraces at different depth (Fig. 11). Channels record the pathways of the upper (UC) and lower (LC) cores of the MOW and the five smaller branches (M1 to M5) defined by Sánchez-Leal et al. (2017) which influence the proximal zone before bottom currents encounter the CDR (Figs. 2 and 11). The MOW cores and their branches interact with the seafloor to shape bottom current depositional and erosional features along the slope (Hernández-Molina et al., 2003, 2014; Llave et al., 2007; Stow et al., 2013).

B) Marginal valleys

Linear and funnel-shaped marginal valleys appear leeward of diapiric ridges and relate to MOW current activity (Fig. 4 and 11). Linear marginal valleys may arise from linear behavior of bottom current filaments formed by secondary circulation (García et al., 2009; Hernández-Molina et al., 2014). Semi-circular and funnel-shaped marginal valleys appear in the cases of features of generally lower elevation relative to the adjacent bottom. In these cases, bottom currents are more vigorous (Fig. 2) with enhanced turbulence that generates erosion in proximal areas adjacent to the ridge and occasional gravitational failures along their flanks (Fig. 11).

C) Sedimentary dunes

The two main types of dune fields exhibit similar morphology and settings indicating they may arise from similar genetic processes. The 3D large and very large dunes appear inside channels and have gravelly sand bottoms with ripples. Steepened lee sides create asymmetric morphologies and different sizes dunes are superposed. Very large 2D dunes appear along the outside margin of channels and marginal valleys. These exhibit sandy mud bottoms without ripples and form symmetric profiles. Dunes decrease in height and increase in wavelength with increasing distance from the edge of the channel/marginal valley.

Relative to 2D dunes, 3D dunes generally form from higher water velocities for a given grain size (Ashley, 1900). These form primarily due to unidirectional current and often exhibit scour pits and curved lee faces (Dalrympie et al. 1978). Sediment transport occurs by the migration of ripples or smaller large-scale bedforms that are superimposed on them (Ashley, 1990). Fields of 3D very large and large dunes in Cádiz and Huelva Channel composed of ripple-marked gravelly sand sediments (Fig. 8g) indicate enhanced bottom current velocities in these locations (Fig. 2).

On the other hand, 2D dunes form due to lower current velocities. The location of these features outside channel margins and marginal valleys confirm this relation. Dune symmetry, especially evident along margins of the funnel-shaped marginal valley leeward of the southern CDR (Fig. 8e), muddy sand sediment composition and the absence of ripples (Fig. 8f) probably indicate oscillatory flow with a zero net transport of sediment (Allen, 1982). Several processes may induce the formation of oscillatory flows in the middle slope of the GoC. Vertical flows over channel margins and marginal valleys represents one such mechanism. The depth of the interphase MOW-ENACW may be strongly stratified and locally course near the seafloor (Sánchez-Leal et al., 2017). This may promote the generation of other oceanographic processes such as internal waves (Hernández-Molina et al., 2016) further indicating oscillatory flow. Internal waves have been evoked to explain the formation of similar dune fields in other areas (Reeder et al., 2011; Belde et al., 2015; Ribó et al., 2016; Droghei et al., 2016). The seismic profile (Fig. 8b) shows increasing dune heights and decreasing wavelengths with depth in the sedimentary record indicating enhanced oscillatory flow with time. This may reflect changes in CDR relief due to tectonic activity. Future research should address the relationship between internal waves and large bedforms in greater detail.

5.2. Substrate diversity and habitat

At a smaller scale, the interaction of bottom currents and fluid venting generates a great variety of substrate and habitat types that can be classified according to bottom current velocity and fluid venting/MDAC formation (Fig. 12). The following sections describe different combinations of these factors.

A) Locations with very low venting and no MDAC formation

In tectonically quiescent areas lacking fluid venting activity, bottom current activity is the main driver of substrate types and habitats. In these cases, the MOW acts as a multicore bottom current that deposits different substrate types (from muddy to gravelly bottoms) to form contourite drifts and their associated erosive features. Present-day bottom current flows produce complex bedform patterns at deciameter to centimeter scales along the seafloor. These remain poorly understood (e.g. Stow et al. 2013; Ercilla et al., 2017) but host substrate types and represent habitats for diverse fauna.

Locations where venting is very low and bottom currents are very weak (c.a. <0.1 m/s) experience higher accumulation of fine grained sediments. Burrowing fauna dominate this mud and sandy mud (MS-BF, Fig. 12). Intense trawling activity affects these deposits because they represent habitat for the Norway lobster (*Nephrops norvegicus*) (González-García et al., 2015).

Settings experiencing slightly higher current intensity (c.a. 0.2-0.35 m/s) host coarser, sandy mud and muddy sand deposits dominated by seapens and other soft-bottom octocorals (e.g. *I. elongata*) (Ms-Oc, fig. 12) as observed between the terminus of the Gusano Channel and Tarsis and Pipoca MVs.

If near-bottom currents increase further to moderate strength (c.a. 0,35-0,5 m/s), deposits become sandier with ripples and may host crinoids such as *Leptometra phallangium*, echinoids (*C. cidaris*) and sea anemones (*A. richardii*) (S-Cr, Fig. 12). Stronger currents (c.a. 0,5-0,6 m/s) can deposit bioclasts but inhibit benthic fauna (S-B, Fig. 12). This substrate and habitat type commonly occurs within the contourite channels as well as in areas of intensive current velocity without channel formation such as areas around Gazul MV which experience the influence of MOW's M5 branch.

B) Locations around venting areas

Interactions between past or present fluid venting processes and currents can transform substrates types from soft to hard bottoms. Microbial activity related to cold seeps control the formation of MDACs through cementation of subsurface permeable layers of fluid-charged sediments (Greinert et al., 2001). The rate and type of past venting activity (e.g. eruptive, diffused, focused) and the action of bottom currents reshaping and exhuming substrates determine present-day morphology of MDACs which includes frequent irregular, massive forms, crusts, boulders, chimneys or fragments of different size (Kopf, 2002; León et al., 2007). The

MDACs in the GoC occur in association with MVs, mud diapirs, fault scarps, along fault-controlled diapiric ridges and also along channels (Magalhaes et al., 2012).

In areas with very high and active venting activity and low bottom current speed (c.a. <0.1 m/s), seafloor deposits consist primarily of fluid-rich mud breccia with microbial mats and chemosymbiotic fauna (Mb-Ch, fig. 12). These features characterize Anastasya MV, the most venting active structure in the study area (Palomino et. al., 2016). Other MVs exhibit lesser degrees of venting activity but are exposed to a stronger bottom current velocities (c.a. 0.3-0.4 m/s). Pipoca MV for example hosts gravelly sediments composed of MDAC fragments with chemosymbiotic communities buried within the first centimeters of the seafloor and heterotrophic communities functioning as mobile suspension feeders (e.g. *L. phalangium*; MX-Ch; Fig. 12).

Areas experiencing extensive and eruptive past venting activity formed massive, irregular MDACs. Added to strong present day bottom currents (c.a. 0.4-0.6 m/s), these settings enable, a rocky substrate with almost no sediment and intensively colonized by large gorgonians like *C. verticillata* and *V. flagellum*. The Chica MV/diapir complex (iM-F, Fig. 12) represents an example of this. Low to moderate currents (c.a. 0.1-0.2 m/s) over massive and irregular MDACs make these carbonates appear semi-buried in muddy sediments and are usually colonized by small sponges along with the occasional large sponge such as *A. setubalense*. The mid sector of the CDR is an example of this (Mm-F, fig. 12).

In areas with a slightly lower past venting activity and stronger present-day bottom currents, MDACs appear mostly as crusts, boulders and chimneys colonized by large suspension feeders. When bottom currents are moderately strong (c.a. 0.3-0.4 m/s), MDACs appear semiburied in sandy sediments with crinoids. Parts of Gazul MV or the CDR's northern sector (Ms-F, Fig. 12) are an example of this. With stronger bottom currents (c.a. 0.4-0.6), MDACs dominate substrates colonized by large suspension feeders (M-F, fig. 12). Areas surrounding extrusional features such as depressions are covered by gravelly sediments consisting primarily of MDAC fragments colonized by solitary corals such as *Flabellum chunii* (MX-sc, Fig. 12).

C) Locations of bioconstructed features

After the formation and exhumation of MDACs and during quiescent periods of limited fluid venting in combination with water mass and current speed conditions, the settlement and growth of CWCs may change pre-existing morphologies and substrate types. These factors contribute to the building of mounds and reefs of up to 100 m in height and several kilometers in length that provide a suitable habitat for many species. Results described here include several confirmed carbonate mounds with abundant coral rubble (Figs. 5c, 7g, 8c and 10c). Topography and backscatter indicate more than 20 additional potential carbonate mounds and crests (Fig. 4).

Cold-water corals in the study area appear in association with venting related features like MVs, diapirs and MV/D complexes. Live scleractinian corals have been found in specific locations as isolated patches such as on the summit and leeward flank of Gazul MV (Palomino et. al., 2016) (CWC-b, Fig. 12). Venting activity at this locality deposits the necessary substrate while bottom currents prevent sedimentation and contribute to favorable conditions for sustained growth of cold-water corals (Wienberg et al., 2009; Rueda et al., 2016; Palomino et al., 2019). In Gazul MV and Geraldine MV/D complex, subsedimentary chemosymbiotic fauna coexist with cold water corals, instead the toxicity of hydrocarbon seepage for corals (Myers and Richardson, 2009; Wehrmann et al., 2011). CWCs grow in these environments when supported by microbially mediated removal of toxic seepage-related substances. The biological buffer maintains favorable conditions for this species (Rincón-Tomás et al., 2019).

Extensive graveyards of CWCs and carbonate mounds with no live corals are widely distributed throughout the area and in other GoC locations (e.g. Faubert et al., 2008; Wienberg et al. 2009; Vandorpe et al., 2017). Several mounds in the GDR's northern sector exhibit coral frameworks colonized by small gorgonians and sponges (CWC-f, Fig. 12). Present day bottom currents are not vigorous enough to prevent sedimentation (Fig. 2). Additionally, seismic profiles show hyperbolic-shaped reflections related to an irregular buried surface reaching 30 m in height (Fig. 5d). Acoustic and morphological similarities with buried coral mounds along the Moroccan margin of the GoC (Faubert et al., 2008; Vandorpe et al., 2017) may indicate the presence of buried mounds. Past conditions of enhanced GoC bottom currents may have favored intensive cold-water coral development (Wienberg et al., 2010).

Nevertheless, the present day MOW expresses very high bottom current velocity at local points along the Spanish margin (Sánchez-Leal et al., 2017), as in CDR's southern sector (c.a. 0.7-0.8 m/s) (Fig. 2). In this area high-resolution seismic profiles show mounds as rounded cone shaped features that crop out along the seafloor (Fig. 8b). These acoustically resemble exposed clusters along the GoC's Moroccan margin (Vandorpe et al., 2017) and the North Atlantic Margin (Mienis et al., 2006; Huvenne et al., 2011). In plan view, these features form a complex of almost parallel and elongated crests 3-4 km in length and up to 40 m in height. Similar to some CWC reefs along the North Atlantic margin (e.g. Mienis et al., 2006; Tong et al., 2012), they strike almost perpendicular to the unidirectional current. Additionally, backscatter values are very high, indicating hard substrates within these mounds. A UCS transect showed large amounts of coral rubble in a valley between two crests (Fig. 8c) and live colonies of *M. oculata* along a flank near the summit (Fig. 8d). Others reports on CWC reefs (Mienis et al., 2006; Tong et al., 2012) have described coarse biogenic material between crests and high densities of living corals at summits. The interaction between the MOW and seafloor may provide more favorable conditions for sustained and healthy CWC growth in these locations.

6. Conclusions

Combination oceanographic, high-resolution multibeam and very high resolution seismic reflection data with surface sediment samples and submarine imagery represents a multidisciplinary approach in detailed mapping morphological features and substrate types along the Gulf of Cadiz margin. These can contribute to a better understanding of interacting geological, oceanographic and sedimentary processes that influence seafloor habitats and biodiversity.

This research identified a hierarchy of processes controlling submarine relief, substrate type and associated habitat. Large scale geological (e.g. regional tectonics, mud diapirism) and oceanographic processes associated with water masses circulation shape the main morphological features (e.g. diapiric ridges, along-slope contourite drifts) while secondary associated geological (gas venting, mud extrusion, MDACs formation, etc.) and oceanographic (cores, branches and filaments, eddies, internal waves, etc.) processes shape smaller seafloor morphological features. These features include erosional (e.g. channels, marginal valleys), depositional (e.g. dunes), extrusional (e.g. mud volcanoes, pockmarks) and bioconstructed (e.g. mounds, reefs) features. At smaller scales, fluid venting activity and bottom currents generate a wide variety of substrate types and habitats and explain the extraordinary geodiversity and biodiversity of GOC's seafloor. Future research concerning the GoC and similar areas can help decode interactions between geological, oceanographic and biological processes and benthic communities.

Acknowledgements

Authors thank colleagues, captains and crew who have participated in the data acquisition during 2010-2019 expeditions aboard R/V Emma Bardán, R/V Cornide de Saavedra, R/V Ramón Margalef and R/V Ángeles Alvariño. This work is supported by INDEMARES/CHICA

(LIFE 07/NAT/E/000732), ISUNEPCA (FB FEP/AC1 20123118_2014; IEO/2015-2017), INTEMARES (LIFE15/IPE/ES/000012), INPULSE (CTM2016 75129 C3 1 R MINECO) and TALUS (CGL2015-74216-JIN) projects. Part of the research was also conducted in the framework of “*The Drifters Research Group*” of the Royal Holloway University of London (UK) and it is related to the projects CTM 2012-39599-C03, CGL2016-80445-R and CTM2016-75129-C3-1-R.

Captions for figures

Figure 1. Study area location. a) Regional bathymetric map of the Gulf of Cádiz (GoC), where the study area (yellow rectangle) is located along the middle continental slope, between 300 and 1000 m water depth (wd) of the Site of Community Importance (SCI) ‘Mud volcanoes of the GoC’ (white polygon). b) Bathymetric map for the study area showing main seafloor features. The location of video stations, sediment samples, and seismic profiles are shown. Black polygons indicate the position of Figures 5 to 10. MV: Mud volcano; MV/D: Mud volcano/diapir complex; D: Diapir.

Figure 2. Regional map (shaded relief) of the study area including the near-bottom instantaneous velocity vectors (black arrows) over a bottom-salinity model (color coded). Modified from Sánchez-Leal et al. (2017). Sectors and zonal divisions are included. CDR: Cádiz Diapiric Ridge, GDR: Guadalquivir Diapiric Ridge.

Figura 3. Main terrain variables used to characterize and map morphological features and substrate types; a) slope; b) aspect, c) broad Bathymetric Position Index (B-BPI); d) fine Bathymetric Position Index (F-BPI); e) backscatter and f) acoustic classes.

Figure 4. Semi-automated geomorphological map based on first order statistics from bathymetric data showing the main morphological features in the study area over a

15x15 m grid cell hillshade map. Sectors and zonal divisions are shown. CDR: Cádiz Diapiric Ridge, GDR: Guadalquivir Diapiric Ridge.

Figure 5. a) Morphosedimentary map of the northern sector of the Guadalquivir Diapiric Ridge (GDR) showing the main morphological features and substrate types. b) The ridge has a flatter summit covered by muddy sand deposits dominated by different seapen species (*Funiculina quadrangularis, Kophobelemnon stelliferum*). Some mounds that outcropping along the bottom are formed by cold-water coral rubble dominated by small-size gorgonians such as *Bebryce mollis* (c). d) Very high resolution seismic profile over the ridge shows the sequence of a contourite drift along the SE flank and a marginal valley along the NW flank. At the top and under the bottom, the seismic profile also shows hyperbolic-shaped reflections related to an irregular buried surface which may indicate the presence of buried mounds.

Figure 6. a) Morphosedimentary map of the mid sector of the Guadalquivir Diapiric Ridge (GDR) showing the main morphological features and substrate types. The ridge appears as two linear and continuous elevations that overlap (b). Over the top the bottom is covered by a variety of sediment with different grain sizes (mainly gravelly northwest flank, subjected to the effects of erosion, shows a bottom formed by rock with coarse sediments (MDACs with irregular massive forms) and colonized by sponges like *Phakellia sp* and similar crinoids(d). Color legend as in Fig. 5.

Figure 7. a) Morphosedimentary map of the northern and mid sectors of the Cádiz Diapiric Ridge (CDR) showing the main morphological features and substrate types. The ridge here looks patched by the action of bottom currents that have eroded a complex system of channels and marginal valleys. This promotes a wide variety of environments at the base, which consist mainly of different types of methane derived

authigenic carbonates (MDACs) like boulders (b), slabs (c) or irregular massive forms with coarse sediments (d, e). The seismic profile (f) shows an area dominated by sedimentation and several mounds formed by MDACs and colonized by large sponges such *Asconema setubalense* (e). Other conical elevations, probably carbonate mounds, are covered by coral rubble (g). Color legend as in Fig. 5.

Figure 8. a) Detailed morphosedimentary map of the southern sector of the Cádiz Diapiric Ridge (CDR) showing the main morphological features and substrate types. The ridge here presents a set of crested mounds on top. In a very high-resolution seismic profile (b) these appear as rounded cone shaped features outcropping on the sea floor. Valleys between crests show large amounts of coral rubble (c) and the foot and flanks show live colonies of *Madrepora oculata* (d). Leeward of the ridge there is a funnel-shaped marginal valley. Seven arc-shaped very large 2D dunes appear at the head of the marginal valley. The sedimentary sequence (e) indicates complex history with the highest heights observed at present. The bottom is covered by sandy mud with high densities of seapens (f). Middle areas of the channel and stoss of the ridge, a very large 3D dune field appears with bottom areas consisting of gravelly sand with ripples and bioclasts (g). Color legend as in Fig. 5.

Figure 9. a) Morphosedimentary map of Gazul MV showing the main features and substrate types. The top as well as the northern and northwestern flanks show seafloor deposits composed of gravels, MDACs and CWC aggregates (mainly *Madrepora oculata*, *Dendrophyllia cornigera* and *Lophelia pertusa*) as well as a wide variety of sponges and other hard substrate fauna (b). Two depressions include several outcrops colonized by hexactinellid sponges (*Asconema setubalense*) as well as by CWCs, gorgonians and other habitat-forming species. In the middle of the depressions, the seafloor is dominated by homogeneous gravelly sand substrate with some solitary

scleractinians (*Flabellum chunii*) (c). d) Morphosedimentary map of Anastasya MV showing the main features and substrate types. The summit is dominated by mud breccia enriched in fluids and organic matter with some microbial mats (e). The summit also shows some patches with boulders and fragmentary MDACs colonized by sponges (f). Color legend as in Fig. 5.

Figure 10. a) Morphosedimentary map of Geraldine MV/diapir complex; b) very high-resolution seismic profile that intersects potential mounds of this structure; c) dredge sample showing mud breccias and abundant coral rubble; d) live colonies of *Lophelia pertusa;* and e) of the antipatharian *Leiopathes glaberrima*. Color legend as in Fig. 5.

Figure 11. 3D sketch showing the regional geological (mud diapirism, regional tectonics) and oceanographic processes (bottom current, water masses). At smaller scales, both geological (mud vulcanism, collapsing) and oceanographic (secondary circulation, vertical eddies, overexcavation, coriolis effects) processes are indicated as well as associated substrate types.

Figure 12. Fluid venting, bottom current dynamics and biological processes can explain the wide diversity of substrate types and habitats in the study area: mud and sandy mud dominated by burrowing fauna (MS-BF); mud and sandy mud dominated by octocorals (MS-Oc); sandy ripples with crinoids (S-Cr); sandy ripples with bioclasts (S-B); cold-water coral framework dominated by small gorgonians (CWC-f); cold-water coral banks (CWC-b); MDACs semiburied in muddy sediments with large suspension feeders (Mm-F); MDACs semiburied in sandy sediments with large suspension feeders (Ms-F); MDACs with large suspension feeders (M-F); mixed sediments with solitary corals (MX-sc); mud breccia with chemosynthesis-based communities (Mb-Ch); mixed sediments with chemosynthetic and heterotrophic

communities (MX-Ch) and irregular massive MDACs with large suspension feeders (iM-F).

References

Allen, J.R.L., 1982. Transverse Bedforms in Multidirectional Flows: Dunes. Developments in Sedimentology 30, Part A, 419-470.

Ashley, G.M., 1990. Classification of large-scale subaqueous bedforms: a new look at an old problem. Journal of Sedimentary Petrology 60 (1), 160-172.

Baringer, M.O., Price, J.F., 1997. Mixing and spreading of the Mediterranean outflow. Journal of Physics Oceanography. 27, 1654–1677.

Belde, J., Back, S., Reuning, L., 2015. Three-dimensional seismic analysis of sediment waves and related geomorphological features on a carbonate shelf exposed to large amplitude internal waves, Browse Basin region, Australia. Sedimentology. 62, 87-109.

Brown, K., Westbrook, G.K., 1988. Mud diapirism and subcretion in the Barbados Ridge accretionary complex: the role of fluids in accretionary processes. Tectonics 7 (3), 613–640.

Bustos, R.A. 2011. Mixing in the Continental slope: study case Gulf of Cádiz. M. Sc. Thesis, University of Liverpool, unpublished.

Camerlenghi, A., Cita, M.B., Della Vedova, B., Fusi, N., Mirabile, L., Pellis, G., 1995. Geophysical evidence of mud diapirism on the Mediterranean Ridge accretionary complex. Marine Geophysical Research 17, 115–141.

Camerlenghi, A. 2018. Drivers of Seafloor Geomorphic Change. In book: Submarine Geomorphology as Benthic Habitat, Editors: Micallef, A., Krastel, S., Savini, A., pp. 135-159.

Carracedo, L.I., Pardo, P.C., Flecha, S., Pérez, F.F., 2016. On the Mediterranean Water Composition. Journal of Physical Oceanography, 46, 1339–1358.

Carter, L., McCave, I.N., 1994. Development of sediment drifts approaching an active plate margin under the SW Pacific deep western boundary undercurrent. Paleoceanography 9 (6), 1061–1085.

Ceramicola, S., Dupré, S., Somoza, L., Woodside, J. 2018. Cold Seeps Systems. In book: Submarine Geomorphology as Benthic Habitat, Editors: Micallef, A., Krastel, S., Savini, A., pp. 367-387.

Cheng, S.C., Hsu, S.K., Wang, Y., Chung, S.H., Chen, P.C., Tsai, C.H., Liu, C.S., Lin, H.S., Lee, Y.W., 2014. Distribution and characters of the mud diapirs and mud volcanoes off southwest Taiwan. Journal of Asian Earth Science, 92, 201-214.

Davies, A.J., Guinotte, J.M., 2011. Global Habitat Suitability for Framework-Forming Cold-Water Corals. PloS ONE 6(4).

Díaz del Río, V., Somoza, L., Martínez-Frías, J., Mata, M.P., Delgado, A., Hernández-Molina, F.J., Lunar, R., Martín-Rubí, J.A., Maestro, A., Fernández-Puga, M.C., León, R., Llave, E., Medialdea, T., Vázquez, J.T., 2003. Vast fields of hidrocarbon-derived carbonate chimneys related to the accretionary wedge/olistostrome of the Gulf of Cadiz. Marine Geology 195, 177–200.

Droghei R., Falcini, F., Casalbore, D., Martorelli, E., Mosetti, R., Sannino, G., Santoleri, R., Chiocci, F. L, 2016. The role of Internal Solitary Waves on deep-water sedimentary processes: the case of up-slope migrating sediment waves off the Messina Strait. Scientific Reports 6, Article number: 36376.

Ercilla, G. Casas, D. Hernández-Molina,F.J., Roque, C., 2017. Generation of Bedforms by the Mediterranean Outflow Current at the Exit of the Strait of Gibraltar. In book: Atlas of

Bedforms in the Western Mediterranean, Editors: Guillén, J., Acosta, J., Chiocci, F.L., Palanques, A., pp. 273-280.

Esentia, I., Stow, E., Smillie, Z., 2018. Contourite Drifts and Associated Bedforms. In book: Submarine Geomorphology as Benthic Habitat, Editors: Micallef, A., Krastel, S., Savini, A., pp. 301-331.

Foubert, A., Depreiter, D., Beck, T., Maignien, L., Pannemans, B., Frank, N., Blamart, D., Henriet, J.P., 2008. Carbonate mounds in a mud volcano province off north-west Morocco: Key to processes and controls. Marine Geology. 248, 74-96.

Faugères, J.C., Mézerais, M.L., Stow, D.A.V., 1993. Contourite drift types and their distribution in the North and South Atlantic Ocean basins. Sedimentary Geology. 82, 189–203.

Fernández-Puga, M.C., Vázquez, J.T., Somoza, L., Díaz del Río, V., Medialdea, T., Mata, M.P., León, R., 2007. Gas-related morphologies and diapirism in the Gulf of Cádiz. Geo-Marine Letters. 27 (2–4), 213–221.

Flinch, J.F., Bally, A.W., Wu, S., 1996. Emplacement of a passive-margin evaporitic allochthon in the Betic Cordillera of Spain. Geology 24 (1), 67–70.

Folk, R.L. 1954. The distinction between grain size and mineral composition in sedimentary rock nomenclature. Journal of Geology, 62 (4), 344-359.

García, M., 2002. Caracterización morfológica del sistema de canales y valles submarinos del talud medio del Golfo de Cadiz (SO de la Península Ibérica): implicaciones oceanográficas. M. Sc. Thesis, Universityof Cadiz, unpublished.

García, M., Hernández-Molina, F.J., Llave, E., Stow, D.A.V., León, R., Fernández-Puga, M.C., Díaz del Río, V., Somoza, L., 2009. Contourite erosive features caused by the Mediterranean outflow water in the Gulf of Cádiz: quaternary tectonic and oceanographic implications. MarineGeology 257, 24–40.

García, M., Hernández-Molina, F.J., Alonso, B., Vázquez, J.T., Ercilla, G., Llave, E., Casas, D. 2016. Erosive sub-circular depressions on the Guadalquivir Bank (Gulf of Cadiz): Interaction between bottom current, mass-wasting and tectonic processes. Marine Geology 378, 5–19.

García-Lafuente, J., Sánchez Román, A., Díaz del Río, G., Sannino, G., Sánchez Garrido, J. C., 2007. Recent observations of seasonal variability of the Mediterranean outflow in the Strait of Gibraltar. Journal of Geophysical Research, 112, C10005.

González-García, E., Rueda, J.L., Bruque, G., López-González, N., Fernández-Salas, L.M., Farias, C., Díaz del Río, V., 2015. Spatial assessment of trawling activity in a shallow mud volcano field of the Gulf of Cádiz, Resúmenes sobre el VIII Simposio MIA15, Málaga del 21 al 23 de septiembre de 2015, Málaga, pp. 377-380.

Greinert, J., Bohrmann, G., Suess, E., 2001. Gas hydrate-associated carbonates and methane-venting at Hydrate Ridge: classification, distribution, and origin of authigenic lithologies. In: Paull, C.K., Dillon, W.P. (Eds.), Natural Gas Hydrates: Occurrence, Distribution and Detection: Geophysical Monograph Series. American Geophysical Union, Washington, pp. 99–113.

Hernández-Molina, F.J., Llave, E., Somoza, L., Fernández-Puga, M.C., Maestro, A., Leoón, R., Barnolas, A., Medialdea, T., García, M., Vázquez, J.T., Díaz del Río, V., Fernández-Salas, L.M., Lobo, F., Alveirinho Dias, J.M., Rodero, J., Gardner, J., 2003. Looking for clues to paleoceanographic imprints: a diagnosis of the gulf of Ca´ diz contourite depositional systems. Geology 31 (1), 19–22.

Hernández-Molina, F.J., Llave, E., Stow, D.A.V., García, M., Somoza, L., Vázquez, J.T., Lobo, F., Maestro, A., Díaz del Río, V., León, R., Medialdea, T., Gardner, J., 2006. The Contourite Depositional System of the Gulf of Cadiz: a sedimentary model related to the bottom current activity of the Mediterranean Outflow Water and the continental margin characteristics. Deep-Sea Research II 53, 1420–1463.

Hernández-Molina, F.J., Llave, E., Preu, B., Ercilla, G., Fontan, A., Bruno, M., Serra, N., Gomiz, J.J., Brackenridge, R.E., Sierro, F.J., Stow, D.A.V., García, M., Juan, C., Sandoval, N., Arnaiz, A., 2014. Contourite processes associated with the Mediterranean outflow water after its exit from the Strait of Gibraltar: global and conceptual implications. Geology 42, 227–230.

Hernández-Molina, F.J., Wåhlin, A., Bruno, M., Ercilla, G., Llave, E., Serra, N., Rosón, G., Puig, P., Rebesco, M., Van Rooij, D., Roque, D., González-Pola, C., Sánchez, F., Gómez, M., Preun, B., Schwenk, T., Hanebuth, T.J.J., Sánchez Leal, R.F., García-Lafuente, J., Brackenridge, R.E., Juan, C., Stow, D.A.V., Sánchez-González, J.M. 2016. Oceanographic processes and morphosedimentary products along the Iberian margins: A new multidisciplinary approach. Marine Geology 378, 127-156.

Huvenne, V.A.I., Beyer, A., Haas, H., Dekindt, K., Henriet, J.-P., Kozachenko, M., Olu-Le Roy, K.,Wheeler, A.J., 2005. The seabed appearance of different coral bank provinces in the Porcupine Seabight, NE Atlantic: results from sidescan sonar and ROV seabed mapping. In: Freiwald, A., Roberts, J.M. (Eds.), Cold-Water Corals and Ecosystems. Springer, Berlin Heidelberg, pp. 535–569.

Kopf, A.J., 2002. Significance of mud volcanism. Reviews of Geophysics, 40(2), 1005.

Lecours, V., Devillers, R., Schneider, D.C., Lucieer, V.L., Brown, C.J., Edinger, E.N., 2015. Spatial scale and geographic context in benthic habitat mapping: review and future directions. Marine Ecology Progess Series, 535, 259-284.

Limonov, A.F., Woodside, J.M., Cita, M.B., Ivanov, M.K., 1996. The Mediterranean Ridge and related mud diapirism: a background. Marine Geology 132, 7–19.

Llave, E., Schönfeld, J., Hernández-Molina, F.J., Mulder, T., Somoza, L., Diaz del Río, V., 2006. High-resolution stratigraphy of the Mediterranean outflow Contourite System in the Gulf of Cadiz during the Late Pleistocene: the impact of Heinrich events. Marine Geology 227 (3–4), 241–262.

Llave, E., Hernández-Molina, F.J., Stow, D.A.V, Fernández-Puga, M.C., García, M., Vázquez, J.T., Maestro, A., Somoza, L., Díaz del Río, V. 2007. Reconstructions of the Mediterranean Outflow Water during the quaternary based on the study of changes in buried mounded drift stacking pattern in the Gulf of Cadiz. Marine Geophysical Research, 28, 379-394.

Llave, E., Matias, H., Hernández-Molina, F.J., Ercilla, G., Stow, D.A.V., Medialdea, T., 2011. Pliocene–Quaternary contourites along the northern Gulf of Cadiz margin: sedimentary stacking pattern and regional distribution. Geo-Marine Letters 31 (5/6).

León, R., Somoza, L., Medialdea, T., González, F.J., Díaz del Río, V., Fernández-Puga, M.C. Maestro, A. Mata, M.P., 2007. Sea-floor features related to hydrocarbon seeps in deepwater carbonate-mud mounds of the Gulf of Cádiz: from mud flows to carbonate precipitates. Geo-Marine Letters, 27, 237-247.

Long, D. 2006. BGS detailed explanation of seabed sediment modified folk classification. Workgroup document of MESHatlantic project.

Maestro, A., Somoza, L., Medialdea, T., Talbot, C.J., Lowrie, A., Vázquez, J.T., Díaz del Río, V., 2003. Large-scale slope failure involving Triassic and Middle Miocene salt and shale in the Gulf of Cadiz (Atlantic Iberian Margin). Terra Nova, 15(6), 380-391.

Maldonado, A., Nelson, C.H., 1999. Interaction of tectonic and depositional processes that control the evolution of the Iberian Gulf of Cadiz margin. MarineGeology 155, 217–242.

Masson, D.G., Wynn, R.B., Bett, B. J. 2004. Sedimentary environment of the Faroe-Shetland and Faroe Bank Channels, north-east Atlantic, and the use of bedforms as indicators of bottom current velocity in the deep ocean. Sedimentology, 51(6), 1207-1241.

Medialdea, T., 2004. Structure and evolution of the "Olistostrome" complex of the Gibraltar Arc in the Gulf of Cádiz (eastern Central Atlantic): evidence from two long seismic cross-sections. Marine Geology 209, 173-198.

Medialdea, T., Somoza, L., Pinheiro, L.M., Fernández-Puga, M.C., Vázquez, J.T., León, R., Ivanov, M.K., Magalhaes, V., Díaz-del-Río, V., Vegas, R., 2009. Tectonics and mud volcano development in the Gulf of Cádiz. Marine Geology 261, 48–63.

Mienis, F., van Weering, T., de Haas, H., de Stigter, H., Huvenne, V., Wheeler, A., 2006. Carbonate mound development at the SW Rockall Trough margin based on high resolution TOBI and seismic recording. Marine Geology 233, 1-19.

Micallef, A., Krastel, S., Savini, A. 2018. Submarine Geomorphology, first ed. Springer Geology, pp. 1-8.

Milkov, A.V., 2000. Worldwide distribution of submarine mud volcanoes and associated gas hydrates. Marine Geology 167, 29–42.

Myers, J. L. and Richardson, L. L. 2009. Adaptation of cyanobacteria to the sulfide-rich microenvironment of black band disease of coral, FEMS Microbiol. Ecol., 67, 242–251.

Nelson, C.H., Baraza, J., Maldonado, A., 1993. Mediterranean undercurrent sandy contourites, gulf of Cádiz, Spain. Sedimentary Geology. 82 (1–4), 103–131.

Nelson, C.H., Baraza, J., Maldonado, A., Rodero, J., Escutia, C., Barber, J.H., 1999. Influence of the Atlantic in flow and Mediterranean outflow currents on Late Quaternary sedimentary facies of the Gulf of Cadiz continental margin. Marine Geology. 155, 99–129.

Palomino, D., Nieves López-González, N., Vázquez, J.T., Fernández-Salas, L.M., Rueda, J.L., Sánchez-Leal, R., Díaz-del-Río, V. 2016. Multidisciplinary study of mud volcanoes and diapirs and their relationship to seepages and bottom currents in the Gulf of Cádiz continental slope (northeastern sector). Marine Geology 378, 196-212.

Palomino, D., Rueda, J.L., Vázquez, J.T., Urra, J., Sánchez-Guillamón, O., González-García, E., López-González, N., Fernández-Salas, L.M. 2019. 24 Cold-Water Corals in Fluid Venting Submarine Structures. In: Orejas C., Jiménez C. (eds) Mediterranean Cold-Water Corals: Past, Present and Future. Coral Reefs of the World, vol 9. Springer, Cham

Pérez-Belzuz, F., Alonso, B., Ercilla, G., 1997. History of mud diapirism and trigger mechanisms in the Western Alboran Sea. Tectonophysics 282, 399–422.

Pinheiro, L.M., Ivanov, M.K., Sautkin, A., Akhmanov, G., Magalhães, V.H., Volkonskaya, A., Monteiro, J.H., Somoza, L., Gardner, J., Hamouni, N., Cunha, M.R., 2003. Mud volcanism in the Gulf of Cadiz: results from the TTR-10 cruise. Mar. Geol. 3269, 1–21.

Platt, J.P., Behr, W.M., Johanesen, K., Williams, J.R., 2013. The Betic-Rif Arc and Its Orogenic Hinterland: A Review. Annual Review of Earth and Planetary Sciences 41, 313-357.

Rebesco, M., Camerlenghi, A., 2008. Contourites, Developments in Sedimentology 60. Elsevier, Amsterdam.

Rebesco, M., Hernández-Molina, F.J., Van Rooij, D., Wåhlin, A., 2014. Contourites and associated sediments controlled by deep-water circulation processes: state of the art and future considerations. Marine Geology 352, 111–154.

Reeder, D.B., Ma, B.B., Yang, Y.J., 2011. Very large subaqueous sand dunes on the upper continental slope in the South ChinaSea generated by episodic, shoaling deep-water internal solitary waves. Mar. Geol. 279, 12-18.

Ribó, M., Puig, P., Muñoz, A., Lo Iacono, C., Masqué, P., Palanques, A., Acosta, J., Guillén, J., Gómez-Ballesteros, M., 2016. Morphobathymetric analysis of the large fine-grained sediment waves over the Gulf of Valencia continental slope (NW Mediterranean). Marine Geology 253, 22-37.

Rincón-Tomás, B., Duda, J.P., Somoza, L., González, F.J., Schneider, D., Medialdea, T., Santofimia, E., López-Pamo, E., Madureira, P., Hoppert, M., Reitner, J., 2019. Cold-water corals and hydrocarbon-rich seepage in Pompeia Province (Gulf of Cádiz) – living on the edge. Biogeosciences, 16, 1607–1627.

Rosas, F.M., Duarte, J.C., Terrinha, P., Valadares, V., Matias, L.,. 2009. Morphotectonic characterization of major bathymetric lineaments in Gulf of Cadiz (Africa–Iberia plate boundary): Insights from analogue modelling experiments. Marine Geology 261, 33-47.

Rueda, J.L., González-García, E., Krutzky, C., López-Rodriguez, F.J., Bruque, G., López-González, N., Palomino, D., Sánchez-Leal, R.F., Vázquez, J.T., Fernández-Salas, L.M., Díaz-del-Río, V. 2016. From chemosynthesis-based communities to cold-water corals: Vulnerable deep-sea habitats of the Gulf of Cádiz. Marine Biodiversity 46:473–482

Sánchez-Leal, R.F., Bellanco, M.J., Fernández-Salas, L.M., García-Lafuente, J., Gasser-Rubinat, M., González-Pola, C., Hernández-Molina, F.J., Pelegrí, J.L., Peliz, A., Relvas, P., Roque, D., Ruiz-Villarreal, M., Sammartino, S., Sánchez-Garrido, J.C. 2017. The Mediterranean Overflow in the Gulf of Cadiz: A rugged journey. Scientific Reports3(11)

Somoza, L., Gardner, J., Díaz-del-Río, V., Vázquez, J.T., Pinheiro, L.M., Hernández-Molina, F.J., TASYO/ANASTASYA shipboard scientific parties, 2002. Numerous methane gas related sea floor structures identified in the Gulf of Cádiz. Eos Trans. AGU 83 (47), 541–549.

Somoza, L., Díaz-del-Río, V., León, R., Ivanov, M., Fernández-Puga, M.C., Gardner, J.M., Hernández-Molina, F.J., Pinheiro, L.M., Rodero, J., Lobato, A., Maestro, A., Vázquez, J.T., Medialdea, T., Fernández-Salas, L.M., 2003. Seabed morphology and hydrocarbon seepage in the Gulf of Cadiz mud volcano area: acoustic imagery, multibeam and ultrahigh resolution seismic data. Marine Geology 195, 153–176.

Stow, D.A.V., Pudsey, C.J., Howe, J.A., Faugères, J.C., Viana, A.R., 2002. Deep-water contourite systems: modern drifts and ancient series seismic and sedimentary characteristics. Geol. Soc. Lond. Mem. 22.

Stow, D.A.V., Faugères, J.C., 2008. Contourite facies and the facies model. In: Rebesco, M., Camerlenghi, A. (Eds.), Contourites, Developments in Sedimentology. 60 Elsevier, pp. 223–256.

Stow, D.A.V., Hernández-Molina, F.J., Llave, E., Bruno, M., García, M., Díaz del Río, V., Somoza, L., Brackenridge, R.E., 2013. The Cádiz contourite channel: sandy contourites, bedforms and dynamic current interaction. Marine Geology 343, 99–114.

Taviani, M., Angeletti, L., Ceregato, A., Foglini, F., Froglia, C., Trincardi, F., 2013. The Gela Basin pockmark field in the strait of Sicily (Mediterranean Sea): chemosymbiotic faunal and carbonate signatures of postglacial to modern cold seepage. Biogeoscience 10, 4653-4671.

Tong, R., Purser, A., Unnithan, V., Guinan, J., 2012. Multivariate Statistical Analysis of Distribution of Deep-Water Gorgonian Corals in Relation to Seabed Topography on the Norwegian Margin. PloS ONE 7(8).

Vandorpe, T., Wienberg, C., Hebbeln, D., van den Berghe, M., Gaide, S., Wintersteller, P., van Rooij, D., 2017. Multiple generations of buried cold-water coral mounds since the Early-Middle Pleistocene Transition in the Atlantic Moroccan Coral Province, southern Gulf of Cádiz. Palaeogeography, Palaeoclimatology, Palaeoecology 485, 293-304.

Wehrmann, L. M. Templer, S. P., Brunner, B., Bernasconi, S. M., Maignien, L., and Ferdelman, T. G. 2011. The imprint of methane seepage on the geochemical record an early diagenetic processes in cold-water coral mounds on Pen Duick Escarpment, Gulf of Cádiz, Mar. Geol., 118–137.

Wienberg, C., Hebbeln, D., Fink, H.G., Mienis, F., Dorschel, B., Vertino, A., Correa, M.L., Freiwald, A., 2009. Scleractinian cold-water corals in the Gulf of Cádiz—first clues about their spatial and temporal distribution. Deep-Sea Research I: Oceanographic Research Papers 56, 1873–1893.

Wienberg, C., Frank, N., Mertens, K.N., Stuut, J.B., Marchant, M., Fietzke, J., Mienis, F., Hebbeln, D., 2010. Glacial cold-water coral growth in the Gulf of Cádiz: implications of increased palaeo-productivity. Earth and Planetary Science Letters 298, 405–416.7.

Yin, S., Hernández-Molina, F.J., Zhang, W., Li, J., Wang, L., Ding, W., Ding, W. 2019. The influence of oceanographic processes on contourite features: A multidisciplinary study of the northern South China Sea. Marine Geology, 415.

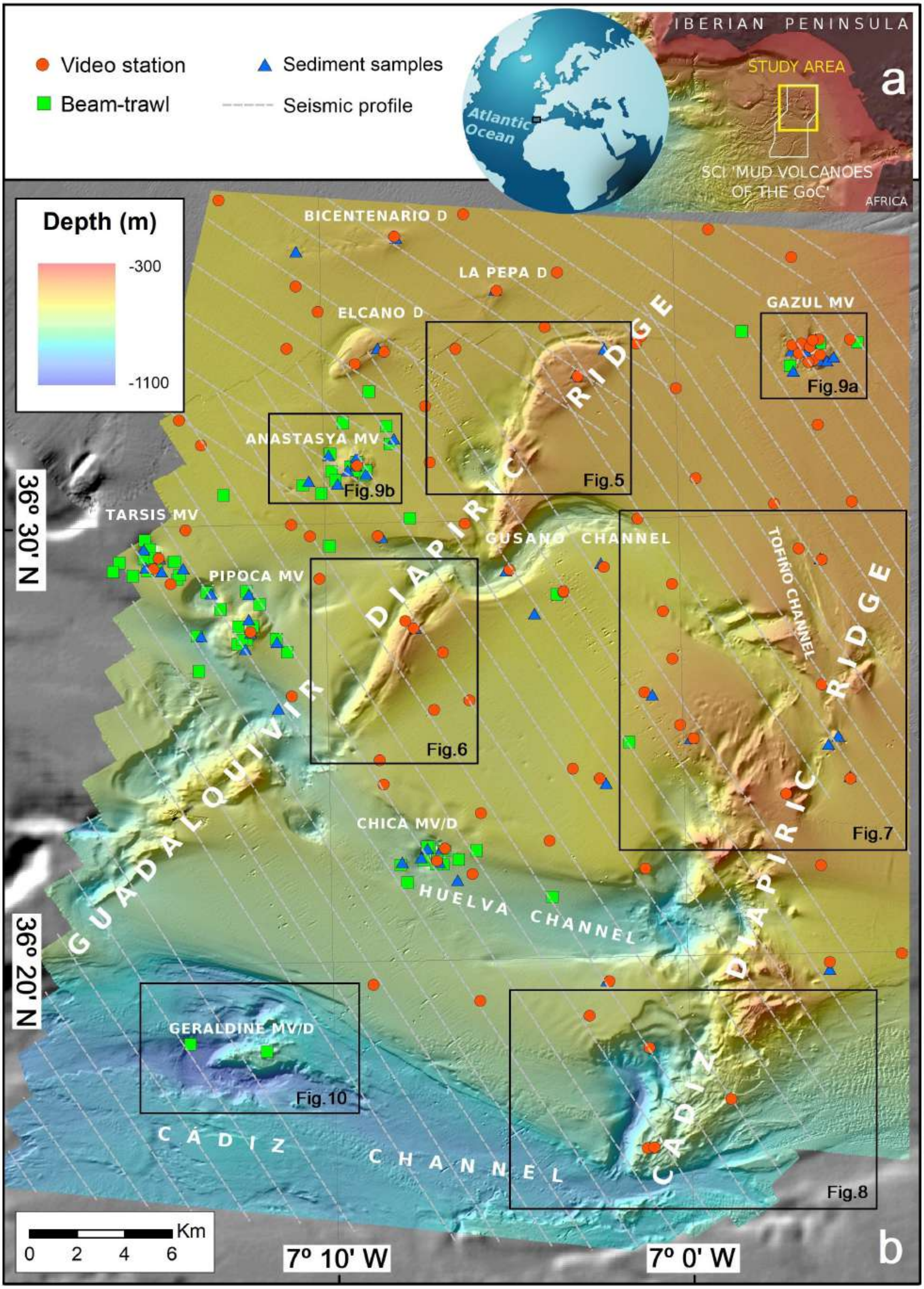

Video station
Beam-trawl
Sediment samples
Seismic profile
Atlantic Ocean
IBERIAN PENINSULA
STUDY AREA
SCI 'MUD VOLCANOES OF THE GoC'
AFRICA
a
Depth (m)
-300
-1100
BICENTENARIO D
LA PEPA D
ELCANO D
GAZUL MV
Fig.9a
ANASTASYA MV
Fig.9b
Fig.5
TARSIS MV
PIPOCA MV
GUSANO CHANNEL
TOFIÑO CHANNEL
DIAPIRIC RIDGE
Fig.6
Fig.7
GUADALQUIVIR DIAPIRIC RIDGE
CHICA MV/D
HUELVA CHANNEL
36° 30' N
36° 20' N
GERALDINE MV/D
Fig.10
CÁDIZ CHANNEL
CÁDIZ DIAPIRIC RIDGE
Fig.8
Km
0 2 4 6
7° 10' W
7° 0' W
b

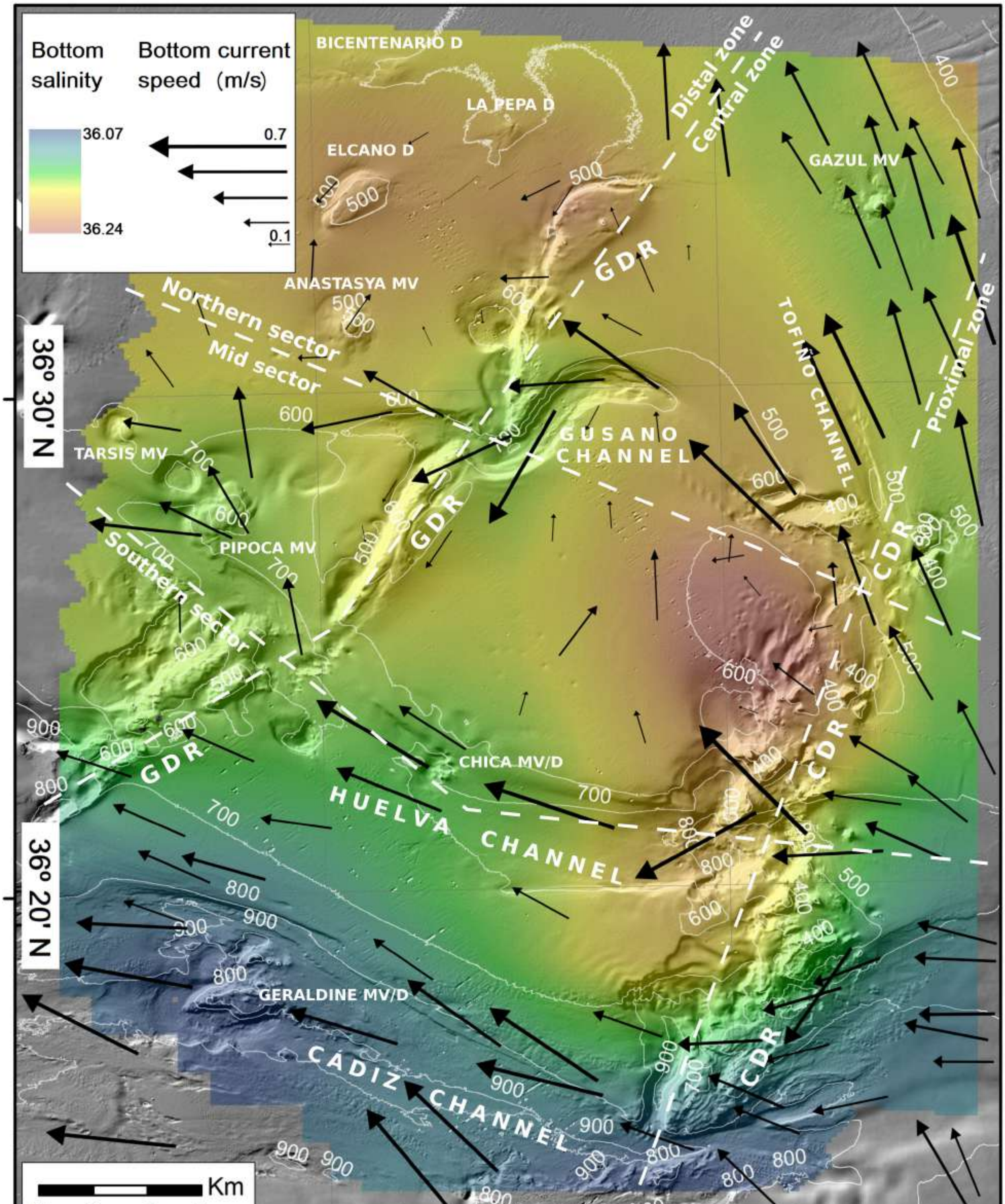

Bottom salinity
Bottom current speed (m/s)
36.07
36.24
0.7
0.1
BICENTENARIO D
LA PEPA D
ELCANO D
ANASTASYA MV
GAZUL MV
TARSIS MV
PIPOCA MV
CHICA MV/D
GERALDINE MV/D
Distal zone
Central zone
Proximal zone
Northern sector
Mid sector
Southern sector
GDR
CDR
GUSANO CHANNEL
TOFIÑO CHANNEL
HUELVA CHANNEL
CÁDIZ CHANNEL
36° 30' N
36° 20' N
7° 10' W
7° 0' W
Km
0 2 4 6

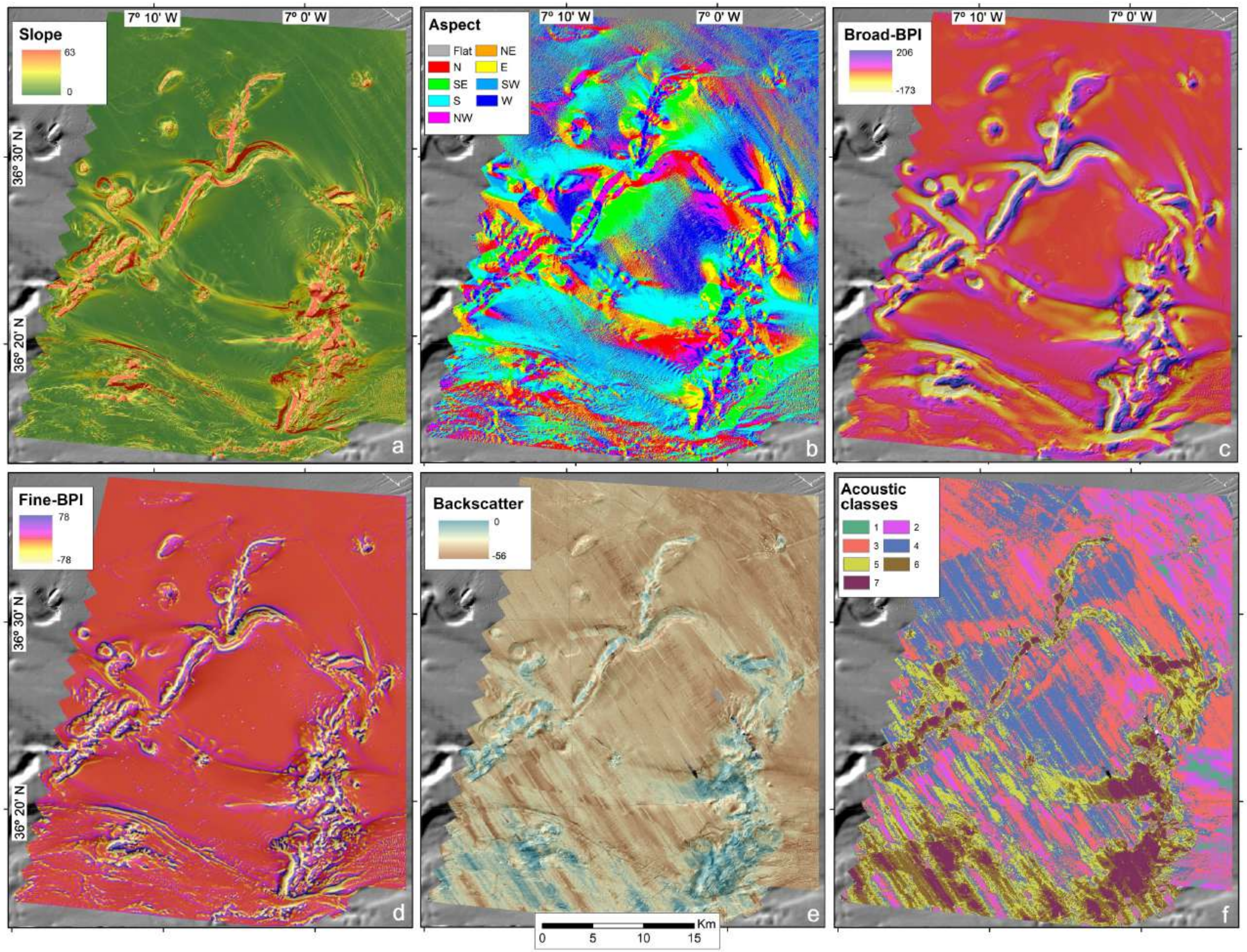

7º 10' W
7º 0' W
36º 30' N
36º 20' N
Slope
63
0
a
Aspect
Flat
NE
N
E
SE
SW
S
W
NW
b
Broad-BPI
206
-173
c
Fine-BPI
78
-78
d
Backscatter
0
-56
e
Acoustic classes
1
2
3
4
5
6
7
f
Km
0
5
10
15

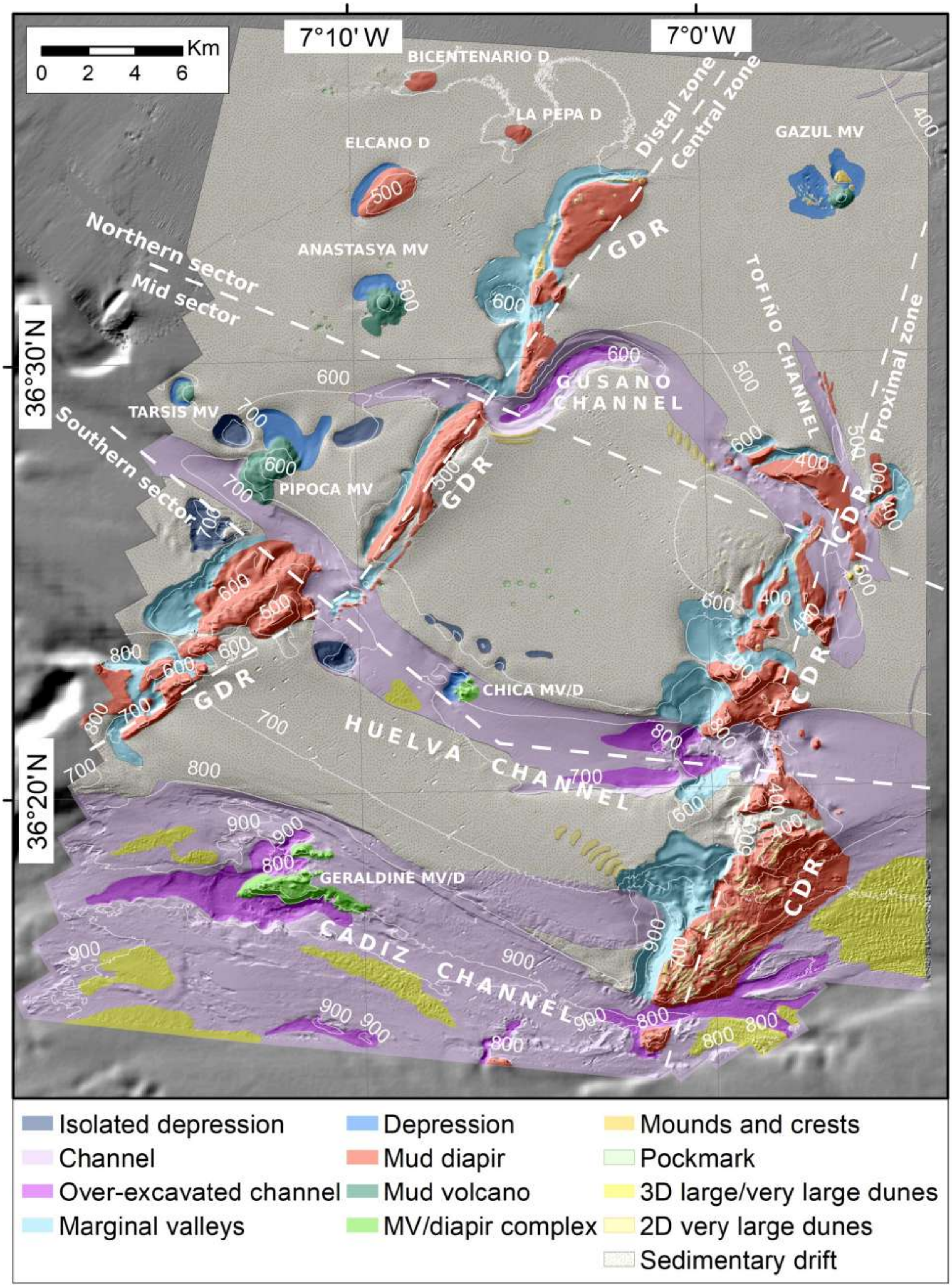

Km
0 2 4 6
7°10' W
7°0' W
36°30' N
36°20' N
BICENTENARIO D
LA PEPA D
ELCANO D
GAZUL MV
ANASTASYA MV
TARSIS MV
PIPOCA MV
CHICA MV/D
GERALDINE MV/D
Northern sector
Mid sector
Southern sector
Distal zone
Central zone
Proximal zone
GDR
CDR
GUSANO CHANNEL
TOFIÑO CHANNEL
HUELVA CHANNEL
CADIZ CHANNEL
Isolated depression
Channel
Over-excavated channel
Marginal valleys
Depression
Mud diapir
Mud volcano
MV/diapir complex
Mounds and crests
Pockmark
3D large/very large dunes
2D very large dunes
Sedimentary drift

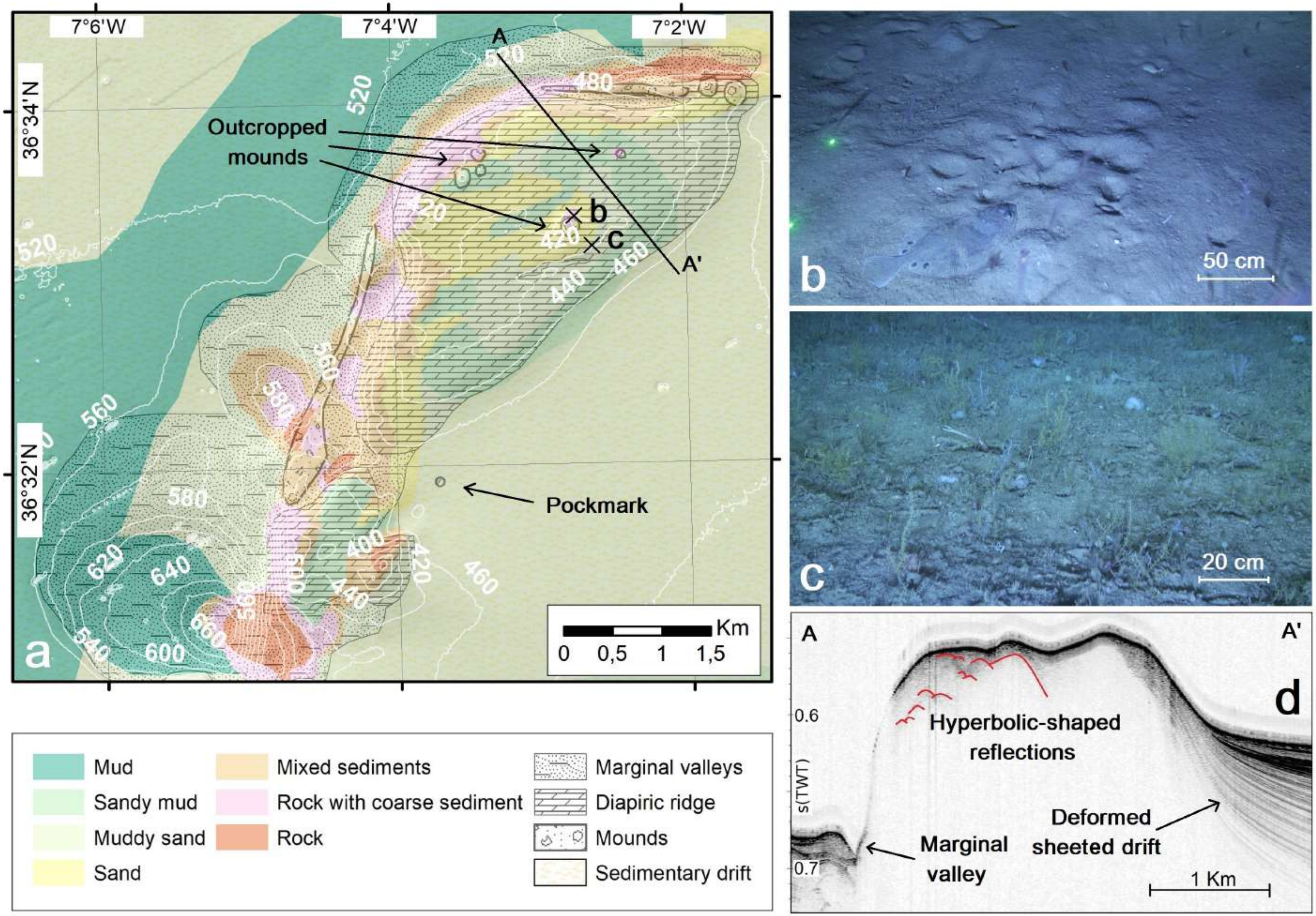
7°6'W
7°4'W
7°2'W
36°34'N
36°32'N
A
A'
Outcropped mounds
b
c
Pockmark
520
480
420
460
440
560
580
620
640
660
540
600
500
400
Km
0 0,5 1 1,5
a
Mud
Sandy mud
Muddy sand
Sand
Mixed sediments
Rock with coarse sediment
Rock
Marginal valleys
Diapiric ridge
Mounds
Sedimentary drift
50 cm
20 cm
A
A'
d
0.6
0.7
s(TWT)
Hyperbolic-shaped reflections
Marginal valley
Deformed sheeted drift
1 Km

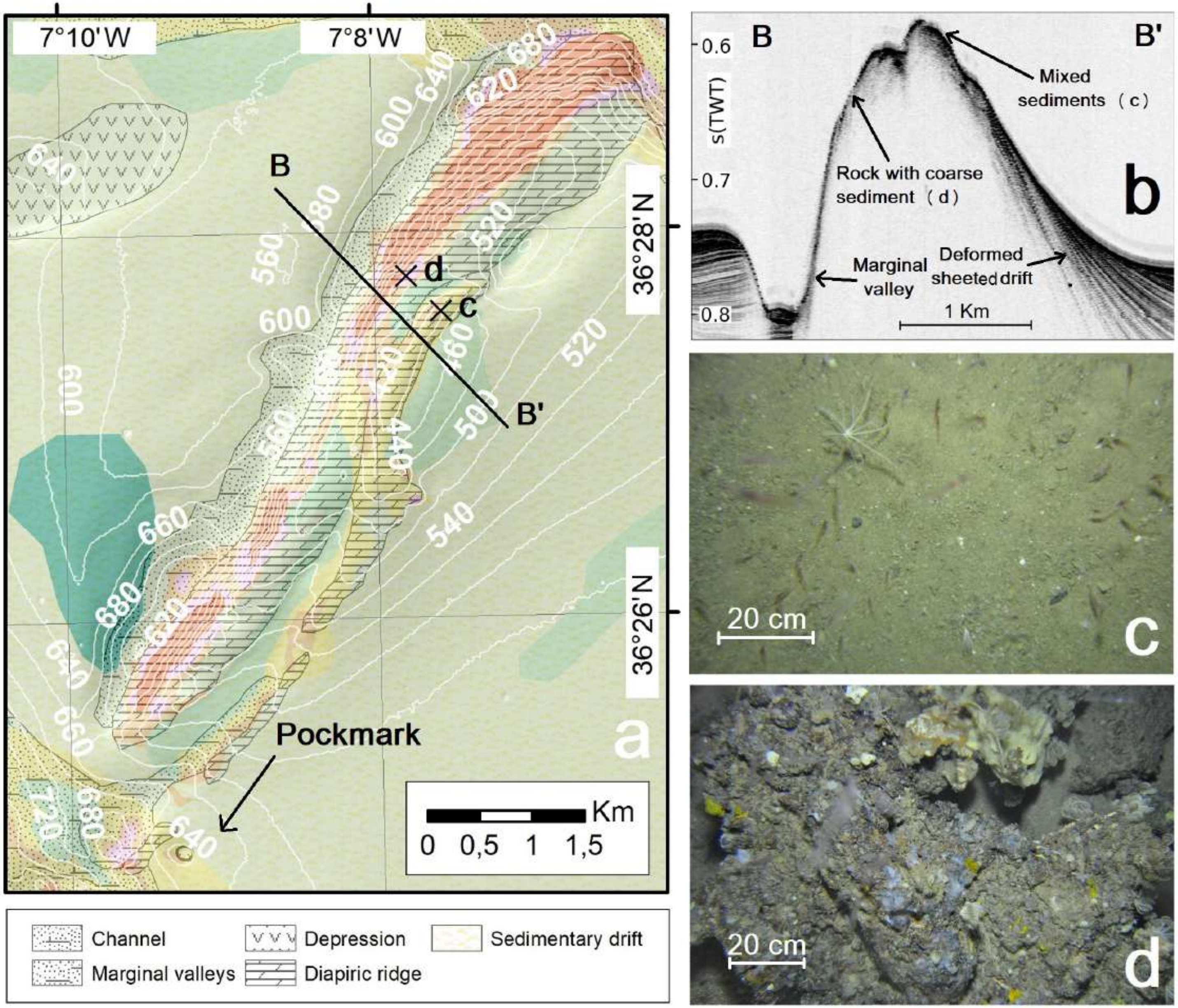

7°10'W
7°8'W
36°28'N
36°26'N
B
B'
d
c
Pockmark
a
Km
0 0,5 1 1,5
Channel
Marginal valleys
Depression
Diapiric ridge
Sedimentary drift
s(TWT)
0.6
0.7
0.8
Mixed sediments (c)
Rock with coarse sediment (d)
Marginal valley
Deformed sheeted drift
1 Km
b
20 cm
c
20 cm
d

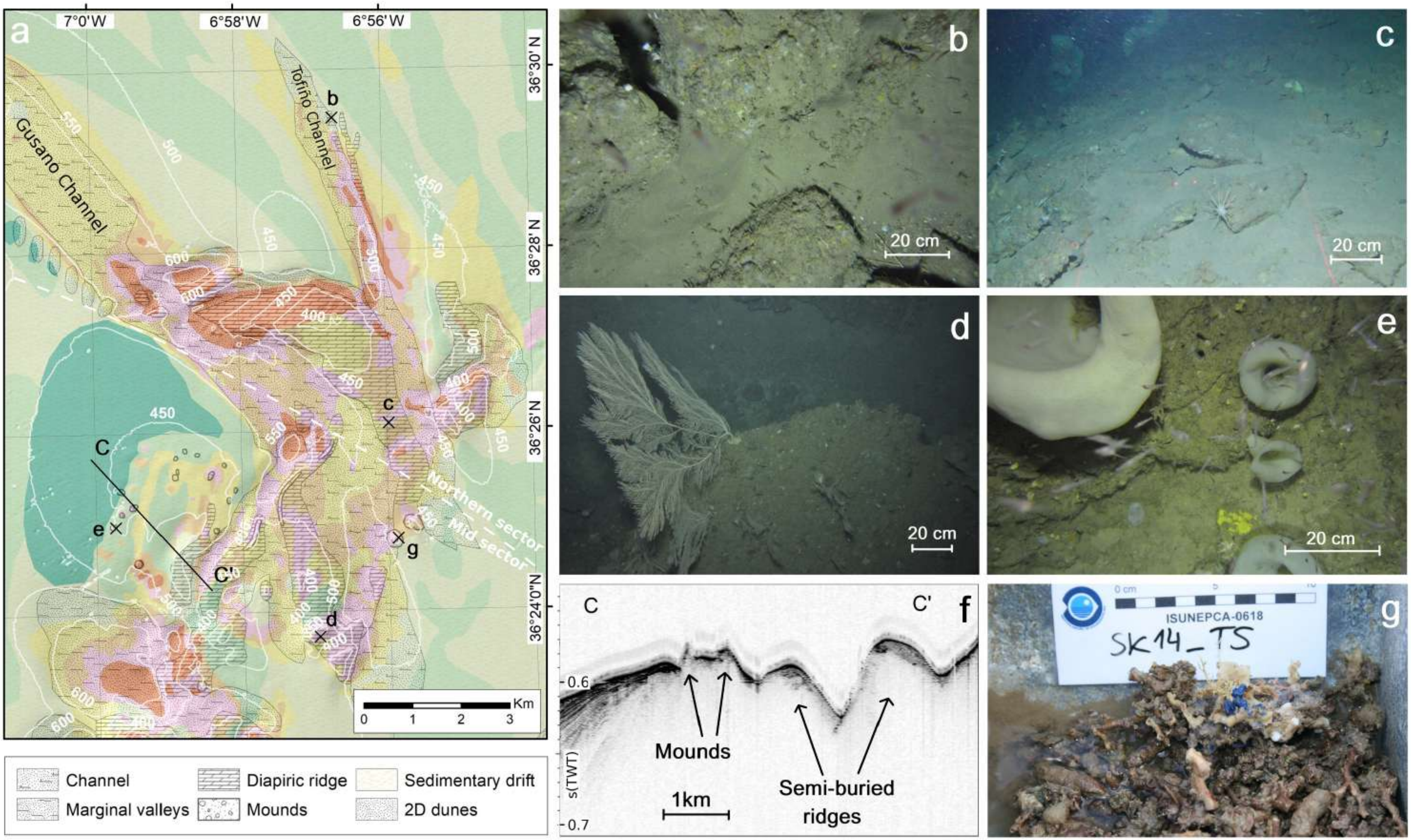

a
7°0'W
6°58'W
6°56'W
36°30'N
36°28'N
36°26'N
36°24'0"N
Gusano Channel
Tofiño Channel
Northern sector
Mid sector
C
C'
Km
0 1 2 3
Channel
Marginal valleys
Diapiric ridge
Mounds
Sedimentary drift
2D dunes
b
c
d
e
20 cm
f
0.6
0.7
s(TWT)
Mounds
Semi-buried ridges
1km
g
ISUNEPCA-0618
SK14_TS

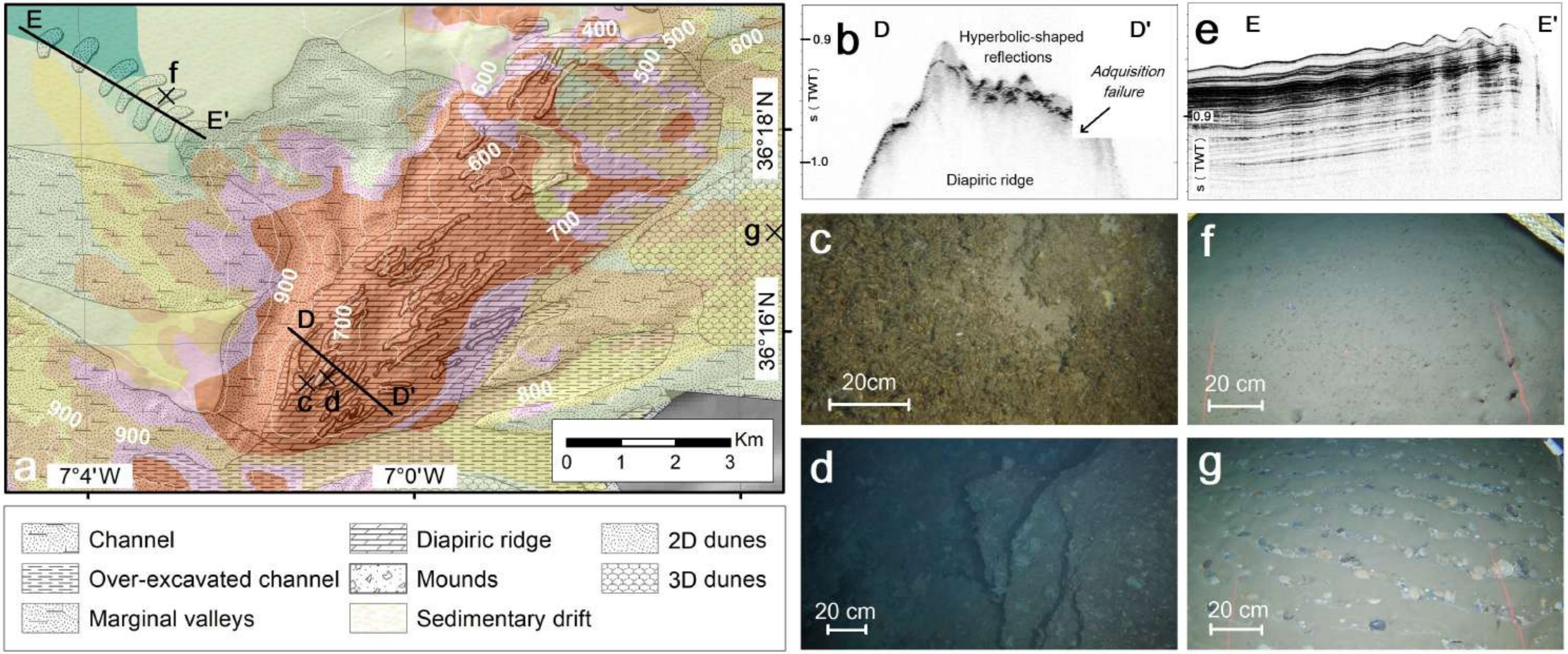

E
f
E'
400
500
500
600
600
600
700
900
700
D
c
d
D'
800
900
900
g
36°18'N
36°16'N
7°4'W
7°0'W
Km
0 1 2 3
a
Channel
Over-excavated channel
Marginal valleys
Diapiric ridge
Mounds
Sedimentary drift
2D dunes
3D dunes
b
D
D'
Hyperbolic-shaped reflections
Adquisition failure
Diapiric ridge
s (TWT)
0.9
1.0
e
E
E'
0.9
s (TWT)
c
20cm
d
20 cm
f
20 cm
g
20 cm

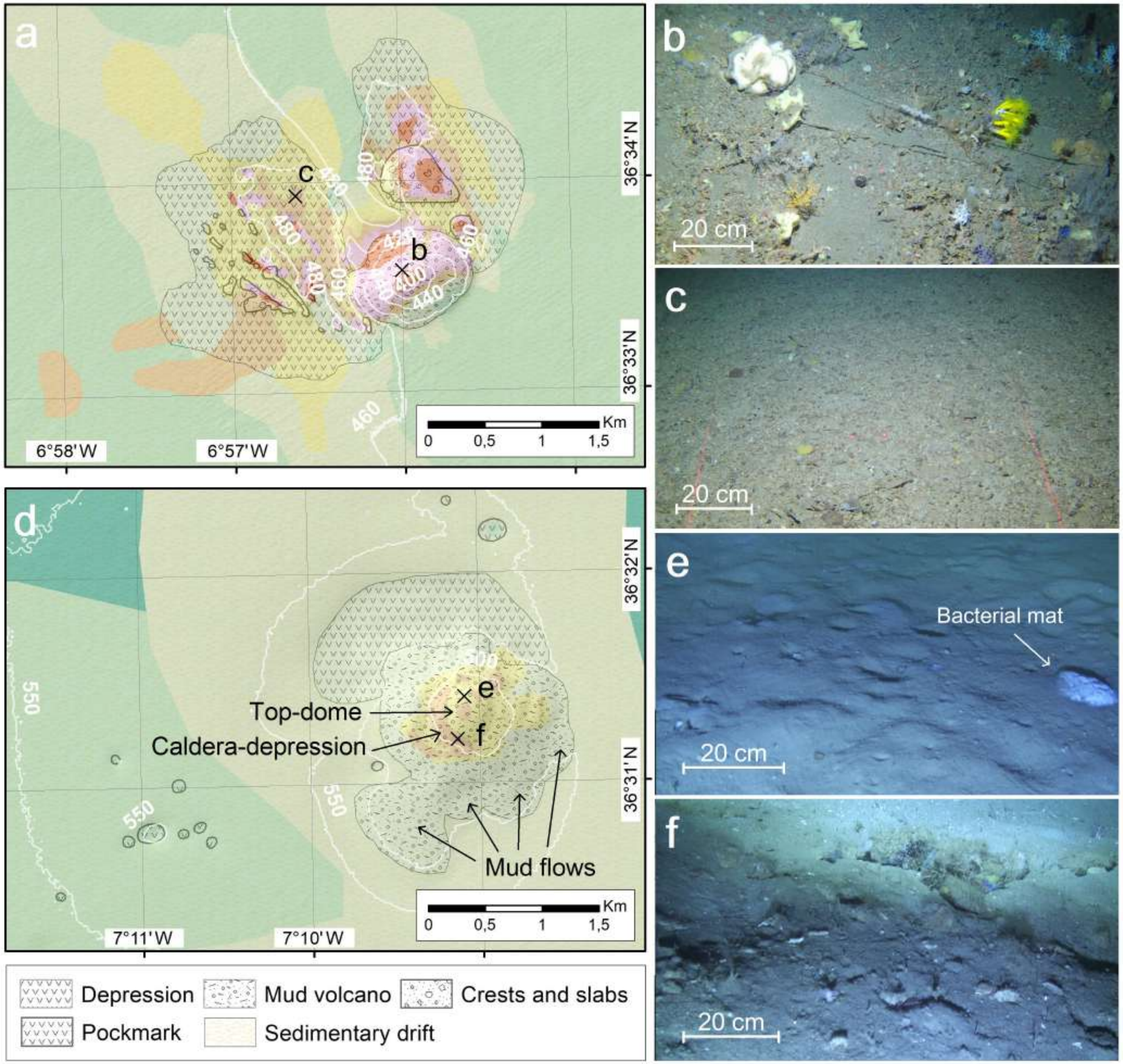
a
b
c
480
460
440
420
400
36°34'N
36°33'N
6°58'W
6°57'W
Km
0 0,5 1 1,5
20 cm
20 cm
d
e
f
Top-dome
Caldera-depression
Mud flows
550
36°32'N
36°31'N
7°11'W
7°10'W
Km
0 0,5 1 1,5
Bacterial mat
20 cm
20 cm
Depression
Mud volcano
Crests and slabs
Pockmark
Sedimentary drift

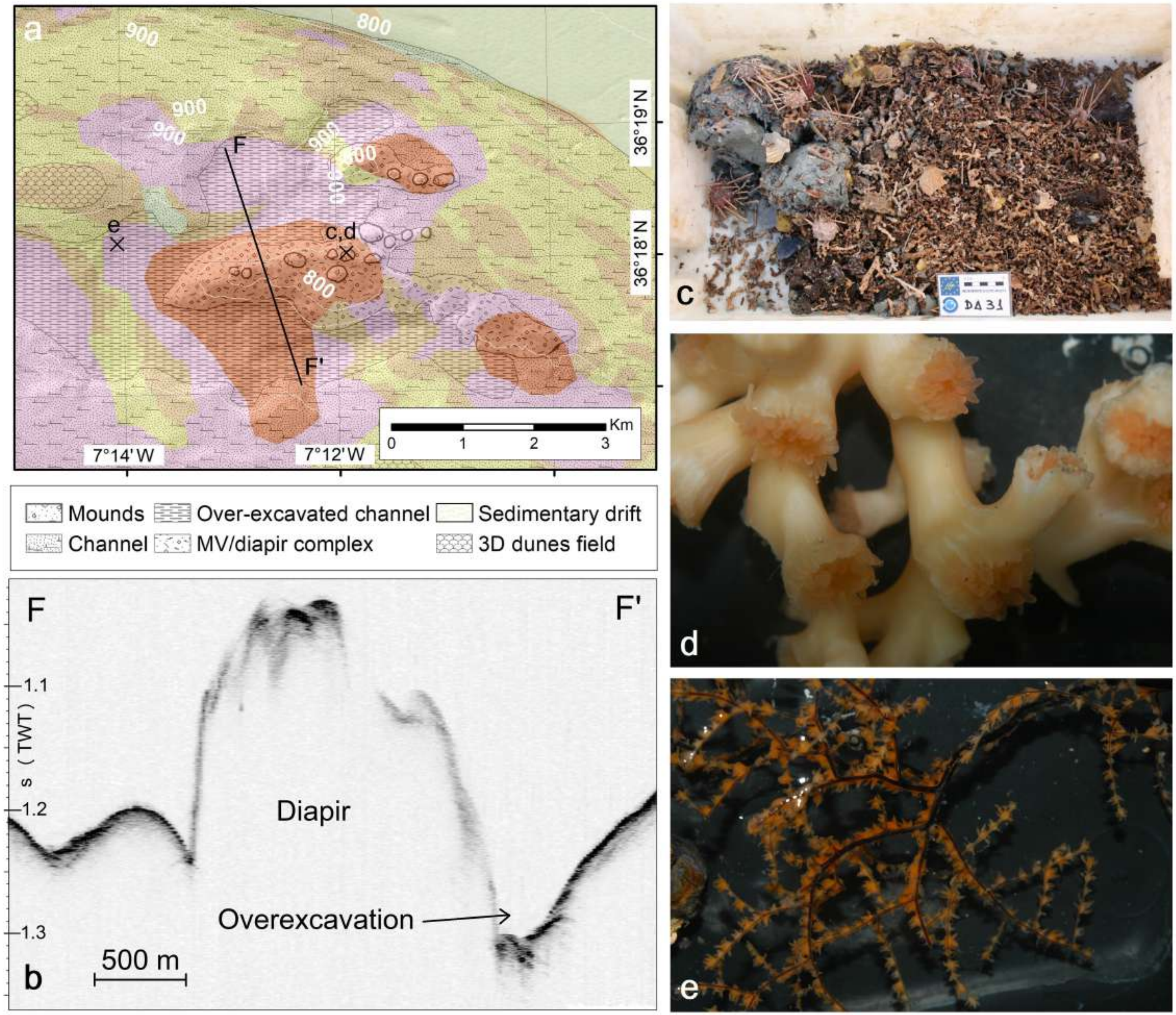
a
900
800
F
F'
c,d
e
36°19'N
36°18'N
7°14'W
7°12'W
Km
0 1 2 3
Mounds
Over-excavated channel
Sedimentary drift
Channel
MV/diapir complex
3D dunes field
b
1.1
1.2
1.3
s (TWT)
Diapir
Overexcavation
500 m
c
DA 31
d
e

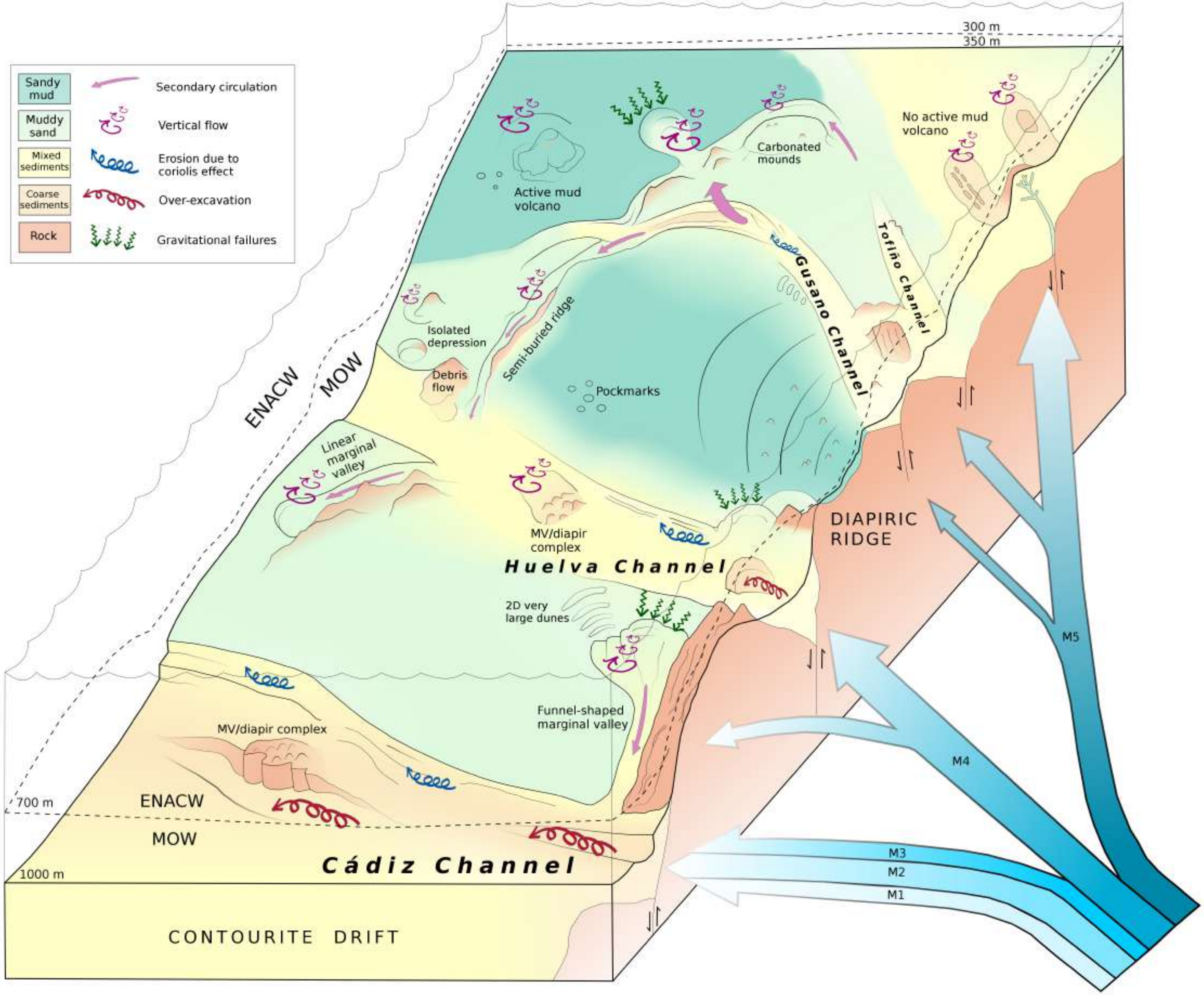

Sandy mud
Muddy sand
Mixed sediments
Coarse sediments
Rock
Secondary circulation
Vertical flow
Erosion due to coriolis effect
Over-excavation
Gravitational failures
300 m
350 m
No active mud volcano
Carbonated mounds
Active mud volcano
Tofiño Channel
Gusano Channel
Isolated depression
Semi-buried ridge
Debris flow
Pockmarks
ENACW
MOW
Linear marginal valley
MV/diapir complex
DIAPIRIC RIDGE
Huelva Channel
2D very large dunes
Funnel-shaped marginal valley
MV/diapir complex
M5
M4
M3
M2
M1
700 m
ENACW
MOW
Cádiz Channel
1000 m
CONTOURITE DRIFT

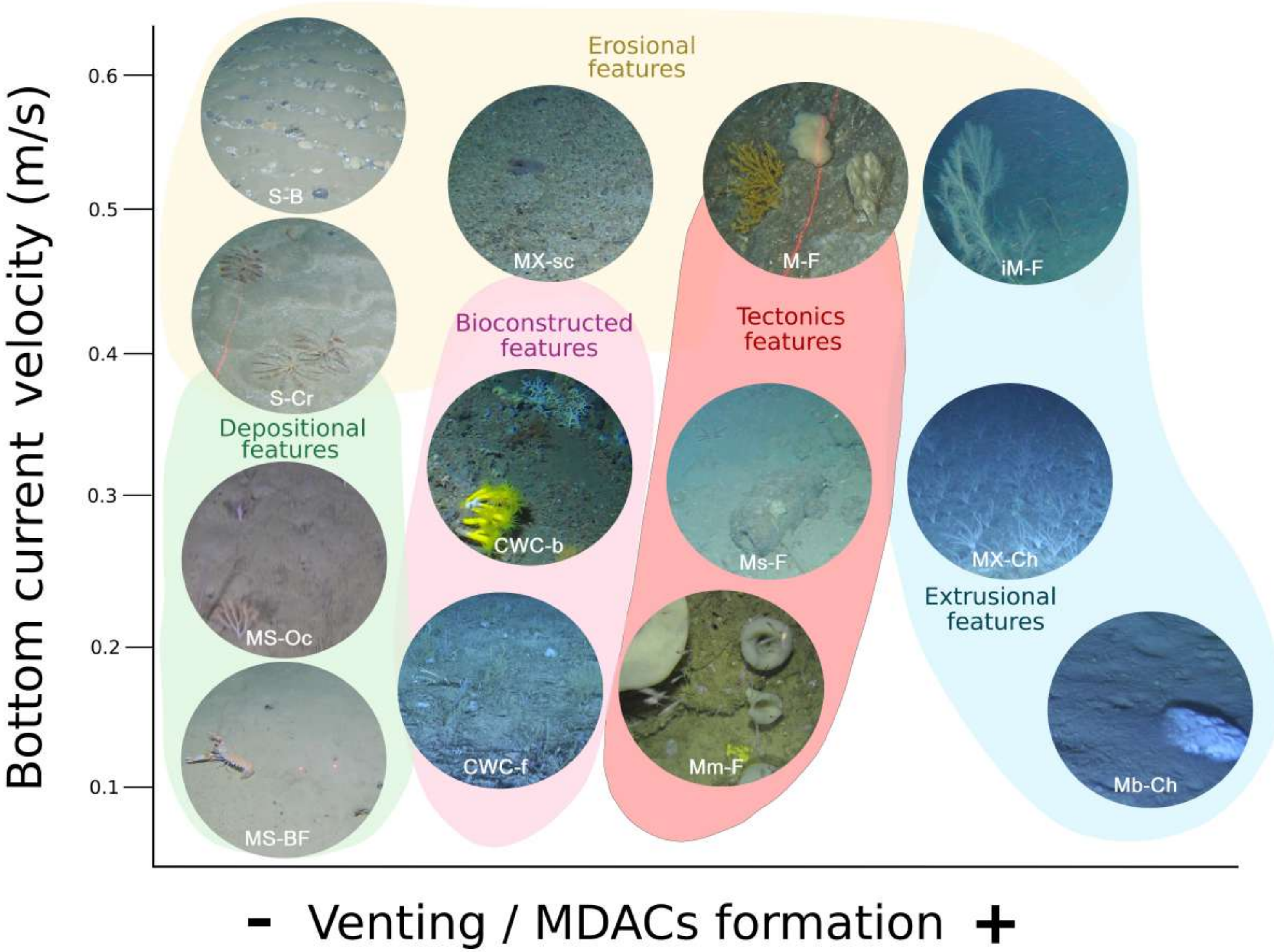

Bottom current velocity (m/s)
0.6
0.5
0.4
0.3
0.2
0.1
Erosional features
Bioconstructed features
Tectonics features
Depositional features
Extrusional features
S-B
S-Cr
MX-sc
M-F
iM-F
CWC-b
CWC-f
Ms-F
Mm-F
MX-Ch
Mb-Ch
MS-Oc
MS-BF
- Venting / MDACs formation +